Renewable Energy 260 (2026) 125194

Contents lists available at ScienceDirect

Renewable Energy

journal homepage: www.elsevier.com/locate/renene

Critical issues for the deployment of floating offshore hybrid energy systems comprising wind and solar: a case study analysis for the Mediterranean Sea

Francesco Superchi, Riccardo Travaglini, Alessandro Bianchini *

Department of Industrial Engineering, University of Florence, Florence, Italy

ARTICLE INFO

Keywords:
Floating photovoltaics
Offshore floating wind
Hybrid energy systems
Optimization

ABSTRACT

Floating offshore energy systems have seen rising attention in recent years. The massive deployment of these systems implies several challenges, especially in sea basins with moderate wind, making floating wind turbines alone not financially viable. In some cases, such as the Mediterranean Sea, the presence of high solar radiation and moderate waves suggests the installation of floating photovoltaic panels, but the integration between different generators with the grid must be carefully evaluated. This study investigates a floating offshore energy system situated near the Sicilian coast, Italy, with a target export capacity of 1 GW. The analysis explores various combinations of wind and solar power to maximize the net present value of the system and minimize the levelized cost of energy, while maximizing the utilization factor of the export cable. In the first scenario, the study considers hybrid farms with a total rated power capacity of 1 GW, varying the wind and solar share in the mix. In the second scenario, solar production is added to a fixed 1 GW wind farm, keeping the maximum power export to shore equal to 1 GW and curtailing the excess. When a high-industry price is considered for floating solar, its levelized cost of energy (137.7 €/MWh) is higher than the remuneration proposed in the 2025 Italian financing scheme (105 €/MWh), making it economically unfeasible in every situation. Results show that the installation cost of solar energy must be lower than 1.11 M€/MWp to be competitive in the current market scenario. Sensitivity analyses on the remuneration applied to both sources go beyond the Italian scenario to show that the hybridization of wind with solar energy in floating systems can improve the techno-economic outcome of the system by exploiting the synergy between the two sources and reducing the cost of the expensive export cable.

1. Introduction

Renewable energy sources (RES) such as wind and solar are spreading all over the world due to their competitive costs, modularity and low emissions. As RES penetration grows, several technical challenges are arising. One of the main issues that must be faced when installing wind turbines or solar panels is related to the intermittency of production.

The problem of producing power in a non-constant way has an even higher economic impact on offshore systems. Energy that is produced in the middle of the sea by offshore generators must be transported to land before being injected into electrical grids. During the construction phase, long and expensive subsea cables must be installed, and they do represent one of the most important cost items [1]. The limited capacity factors characterizing wind and solar energy production may lead to a limited utilization factor of this export cable, thus reducing the depreciation of the initial expense.

To address this problem, the combination of wind and solar energy (in the form of floating photovoltaic panels, FPV) is gaining increasing attention due to their complementary nature.

Morin et al. [2] specifically studied the wind and solar integration during periods of low renewable generation (RES droughts), in onshore environments. They found out that the addition of solar capacity to wind systems results in a significant reduction of frequency and duration of RES droughts. Yuan et al. [3] compared the complementarity between wind and solar in onshore and offshore environments in East Asia. They found that hourly complementarity is strong between offshore resources, but weaker on a daily scale.

Vázquez et al. [4] evaluated the effectiveness of combining solar, wind, and waves on the Spanish coasts. The authors claim that the use of hybrid platforms would not only increase energy production but also

* Corresponding author.
E-mail addresses: francesco.superchi@unifi.it (F. Superchi), riccardo.travaglini@unifi.it (R. Travaglini), alessandro.bianchini@unifi.it (A. Bianchini).

https://doi.org/10.1016/j.renene.2026.125194
Received 22 August 2025; Received in revised form 21 November 2025; Accepted 3 January 2026
Available online 4 January 2026

Nomenclature

A	Area of PV modules
AEP	Annual Energy Production
CAPEX	Capital Expenditures
CF	Capacity Factor
COBYLA	Constrained Optimization BY Linear Approximation
DHI	Diffuse Horizontal Irradiance
DNI	Direct Normal Irradiance
d_r	Inter-row spacing
DR	Rotor diameter
E	Energy
FB	Fixed-bottom
FL	Floating
FPV	Floating Photovoltaics
FWT	Floating Wind Turbine
GHI	Global Horizontal Irradiance
HL	Humidity Losses
i	Discount Rate
I_0	Initial investment cost
L	Length of solar panels
LCOE	Levelized Cost of Energy
n	Project lifetime in years
NOJ	Niels Otto Jensen wake model
NPV	Net Present Value
NSRDB	National Solar Radiation Database
ON	Onshore
OPEX	Operating Expenditure
P	Power
PBT	Payback time
POA	Plane of Array
PV	Photovoltaics
R	Remuneration
RES	Renewable Energy Sources
SWH	Significant Wave Height
T	Temperature
U	Heat loss coefficient
UF	Utilization Factor
w	Wind speed
WIL	Wave-Induced Losses
WT	Wind turbine

Greek symbols

β	Tilt angle of panels
α	Absorption coefficient
γ	Temperature coefficient
η	Efficiency

Subscripts

a	air
c	cell
fix	fixed
irr	irradiance
m	module
v	dependent on wind speed
var	variable
STC	Standard Test Conditions

reduce its variability.

Wind and solar combination in offshore environments can even reduce the environmental impact of large energy systems, increasing the power density of farms. López et al. [5] performed a technical analysis regarding a combined floating offshore wind and FPV system located in Asturias (Spain). Their results showed that hybrid configurations are able to reduce power output variability throughout the year with respect to single-source systems. Jiang et al. [6] assessed the offshore floating wind-solar energy potential in China and demonstrated that co-located farms diminish generation variability. Ali et al. [7] also highlighted that co-located wind and solar projects can reduce cost components associated with offshore renewables.

Costoya et al. [8] also studied the combination of floating offshore wind and solar PV to stabilize the energy supply. Their results confirmed that wind-solar farms improve the resource by reducing the spatial and temporal variability of both individual energy resources. Bi and Law [9] studied the effects of high wind and wave conditions on solar power performance in co-located offshore wind and solar farms. Results of their simulations show that PV output would remain stable even under conditions that may challenge wind generation. De Souza Nascimento et al. [10] studied the complementarity of floating offshore wind and solar in Brazil and observed that, in some cases, solar can complement offshore wind up to 40 %.

Frías-Paredes and Gastón-Romeo [11] proposed a new methodology to evaluate the complementarity of resources during the design phase of floating wind and solar hybrid energy systems and identify the most suitable areas for the promotion of these combinations. Liu et al. [12] proposed a three-step framework for optimal site selection of offshore wind-PV-wave-hydrogen energy systems that can be used as a reference for the implementation of offshore projects.

Despite these advantages, results from the literature review by Khurshid et al. [13] highlight a lack of research on true cost estimation of systems mixing solar energy with wind and wave energy. Huang and Iglesias [14] tried to determine the optimum solar capacity to be added to a certain installed wind energy capacity for fixed-bottom offshore wind farm retrofitting with FPV, aiming primarily at reducing power production variability. They found that the expected installed solar capacity (118–887 MW) should be slightly larger than that of the wind farm (102–603 MW).

Jahangir et al. [15] performed a feasibility study of a hybrid system comprising onshore wind and PV combined with wave energy for coastal cities. They obtained favorable results from the application of this combination (2–9.2 MW wind plus 7.2–14.4 MW solar), as in another study by some of the same authors [16] considering a similar system (1.25–2.5 MW onshore wind plus 3.6–8 MW FPV). Kumar et al. [17] presented a multi-objective optimization for a hybrid offshore system with electrical and hydrogen loads comprising FPV (5–24 MW) and fixed-bottom wind turbines (0.8–1 GW), and supported by batteries and hydrogen, aiming at satisfying electrical and hydrogen loads.

Furthermore, current offshore wind farms may also benefit from the installation of additional solar power. Indeed, the specific capacity of the export cable that connects the offshore wind farms to the onshore grid is not fully used due to the limited capacity factor of the wind farm. The act of sharing the same export cable to bring to shore both solar and wind energy can be referred to as “cable pooling”.

Delbeke et al. [18] studied the complementarity of fixed-bottom offshore wind and FPV in the Belgian North Sea. Their results show that the highest degree of complementarity between the two sources is found on monthly and weekly timescales, while it is less pronounced in shorter frames as daily, hourly, or 10-min timescales. The authors also studied the integration of 3020 MWp of FPV on top of 2262 MW of offshore wind, limiting the cable export capacity to 2254.4 MW. Their results show that the additional FPV would increase the renewable electricity yield by 47 %, while curtailing around 16 % of the PV output and raising the cable capacity factor from 37 % to 50 %.

Golroodbari et al. [19] performed a techno-economic study on the integration of FPV (up to 1.9 GW) within a 752 MW offshore fixed-bottom wind farm in the North Sea under the constraint of a certain fixed cable capacity of 700 MW. Even if the introduction of solar energy led to higher energy exports, the NPV of hybrid systems was lower than the wind-only base scenario in the absence of subsidies.

Kazemi-Robati et al. [20] also proposed a stochastic optimization framework to hybridize offshore fixed-bottom and floating wind farms (25.2–60 MW) with wave energy (0–74 MW) and FPV (107–147 MW), considering the cable export limitation (50–80 MW) in three locations. The authors concluded that combining different energy sources brings economic profit, and curtailment due to export limits remains at reasonable percentages.

1.1. Research gaps and contribution

The present work contributes to the literature by considering a fully floating hybrid system installed in an offshore environment. All components are simulated using engineering models, considering the effect of key phenomena on the performance of generators (i.e., wake losses for wind turbines and wave and humidity losses for floating solar panels).

Table 1 reports a literature review of studies on offshore wind-solar hybrid systems. Many studies on floating offshore systems have focused only on the technical aspects of combining wind and solar energy. On the other hand, only a few studies delved into the financial feasibility of these combinations. Since the FPV technology is still in the early stages of development, there is an inherent need to study its economic effectiveness in expected energy markets. Moreover, due to the uncertainty behind the actual installation cost and the possible remuneration applied to this novel technology, sensitivity analyses are required to understand under which market conditions FPV can be economically viable.

Governments and institutions have started proposing new remuneration for floating generators, but without a fair comparison with their actual production costs, these new technologies may be unable to enter the market. Some previous studies have assumed market prices based on future projections. This study proposes instead a techno-economic assessment of an actual case study, based on a real remuneration framework proposed in a recent decree, the “FER2”.

Another point of novelty is represented by the geographical positioning of systems considered in previous studies, which focused on systems installed in Ocean environments. Differently, this work considers the typical conditions characterizing the Mediterranean area, i.e., lower wind capacity factors, higher PV capacity factors, and a new remuneration scheme.

This paper aims to present not only the technical benefits that the combination of solar and wind energy can bring to the electricity mix but also give some critical insights into the financial outcome that these systems would have under an actual remuneration scheme proposed in a European country like Italy.

2. Case study

Fig. 1 shows a graphical representation of the connection and components present in the wind-solar floating system considered, highlighting the presence of the shared electrical substation between wind and solar floating generators and the single cable connection to the onshore substation.

The case study is located approximately 60 km from the western shores of Sicily, where previous feasibility projects were presented to the Italian authorities [21].

The offshore hybrid system is characterized by a maximum output power of 1 GW, in two scenarios.

- **1st scenario**: installation of a hybrid system characterized by a total rated power of 1 GW. Several configurations involving an increasing number of 15 MW wind turbines are considered (one to sixty-seven), while the solar installation is tailored to reach the total target size. Results from this scenario show which is the optimal wind and solar mix to minimize the LCOE, maximize NPV, and what is the effect on the overall performance of the system.
- **2nd scenario**: installation of a hybrid farm again with a maximum export capacity of 1 GW but comprising a 1-GW floating offshore wind farm (sixty-seven 15 MW wind turbines) and additional solar capacity. This time, the 1-GW export cable allows for the export of solar energy only when PV production happens during instances of low wind production. Solar energy is instead curtailed when the total energy production of the hybrid farm exceeds the rated level. Results from this scenario help to understand if solar energy may support the wind farm in better exploiting the export cable.

3. Methods

This section first describes the input data required to estimate the solar and wind production of the hybrid configuration under analysis. Then, it details the modeling approach for both the FPV and the FWTs involved and how the power flows are managed in the hybrid system. Finally, the main techno-economic assumptions and the metrics used to evaluate the overall performance of different configurations are presented.

Table 1
Literature review of studies on wind-solar hybrid systems, differentiating between systems comprising onshore (ON), offshore fixed bottom (FB) or offshore floating (FL) wind.

Study	Location	WT type	WT [MW]	PV [MWp]	Cable [MW]	Analysis	Market price	Cable pooling
[3]	East Asia	-	–	–	–	Technical	–	No
[4]	Spain	–	–	–	–	Technical	–	No
[5]	Atlantic Ocean (Spain)	FL	6.2	5	–	Technical	–	No
[6]	Pacific Ocean (China)	FB, FL	–	1.11	–	Techno-economic	–	No
[8]	Atlantic Ocean (Iberian Peninsula)	FL	–	–	–	Technical	–	No
[9]	Pacific Ocean (China)	–	–	–	–	Technical	–	No
[10]	Atlantic Ocean (Brazil)	FL	–	–	–	Technical	–	No
[11]	Atlantic Ocean (Iberian Peninsula)	FL	–	–	–	Technical	–	No
[14]	North Sea and Pacific Ocean (China)	FB	102–603	118–887	–	Technical	–	No
[15]	Caspian Sea, Persian Gulf, and Gulf of Oman	ON	2–9.2	7.2–14.4	–	Techno-economic	Assumed	No
[16]	Caspian Sea and Persian Gulf	ON	1.25–2.5	3.6–8	–	Techno-economic	Assumed	No
[17]	Pacific Ocean (Australia)	FB	885–1000	5–24	–	Techno-economic	–	No
[18]	North Sea	FB	2262	500–3500	2254.4	Technical	–	Yes
[19]	North Sea	FB	752	0–1900	700	Techno-economic	Assumed	Yes
[20]	North Sea and Atlantic Ocean	FB, FL	25.2–60	107–147	50–80	Techno-economic	Assumed	Yes
Present study	Mediterranean Sea	FL	0–1005	0–2000	1000	Techno-economic	Actual	Yes

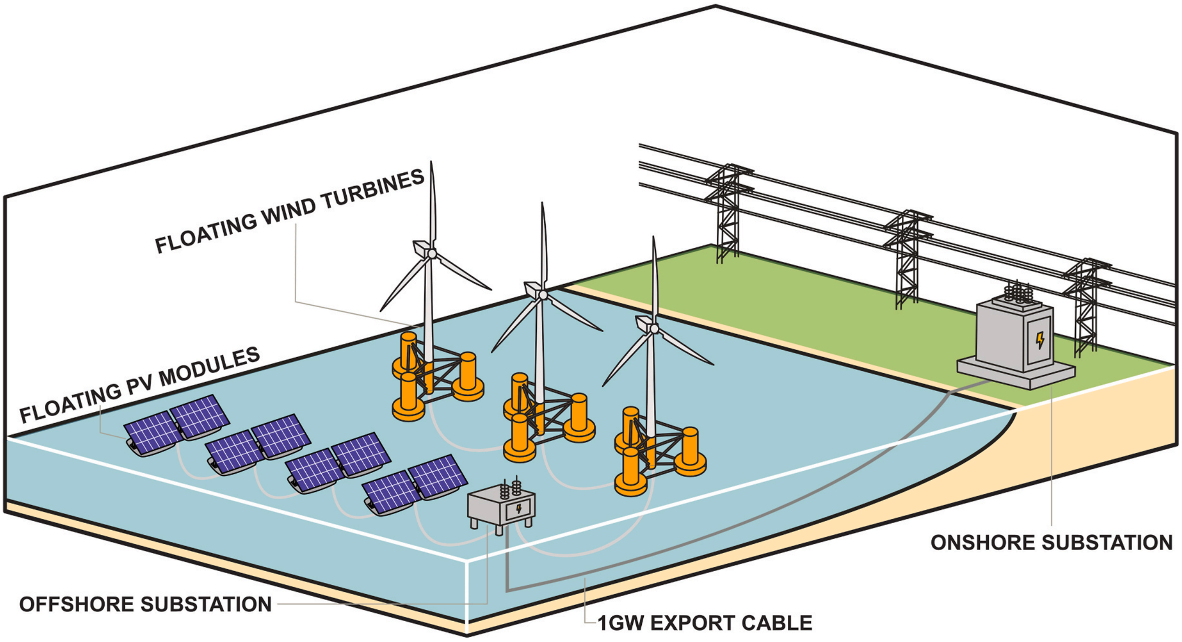

Fig. 1. Graphical representation of the components and connections present in a wind-solar floating offshore system.

3.1. Solar data

The FPV model requires several inputs. A typical meteorological year with a 1-h time resolution was obtained from the National Solar Radiation Database (NSRDB) for the selected location. The typical year was generated starting with data from 2014 to 2022. This dataset contains the time series of Global Horizontal Irradiance (GHI), Direct Normal Irradiance (DNI), and Diffuse Horizontal Irradiance (DHI). Moreover, the dataset contains the air temperature and the wind speed at 2m height. Figure A 1 in the Appendix shows the yearly trend of GHI, DNI, and DHI during the typical year (a) and a zoom over three weeks (b).

For the time-dependent analysis required to study the second scenario (as described in Section 2), in which solar power is curtailed when the production exceeds the maximum export capability of the cable, the solar dataset was linearly interpolated to match the 10-min time resolution of the wind dataset. Even if this approach limits the representation of intra-hour variability, it was necessary due to the absence of solar measurements at 10-min resolution and represented the best feasible option with the data available.

3.2. Wind data

A Weibull distribution describing the wind resource at 100 m above sea level in the selected location was obtained from ERA5 and used for layout optimizations. Fig. 2 shows the corresponding distribution of wind speeds and the wind rose for the selected site. The overall distribution is represented by the black line on the left, while the energetic contents from twelve different directions are represented by the dashed colored lines. The wind rose on the right displays the energetic content from the different directions using polar coordinates. The resource was then extrapolated at hub height (150m) following a procedure described in section 3.4.

For the time-dependent analysis, a time-varying dataset of the wind speed was retrieved from ERA5 for the years 2018 and 2019. In order to account for the power production variability while respecting the applicability range of the power curve of wind turbines, the time

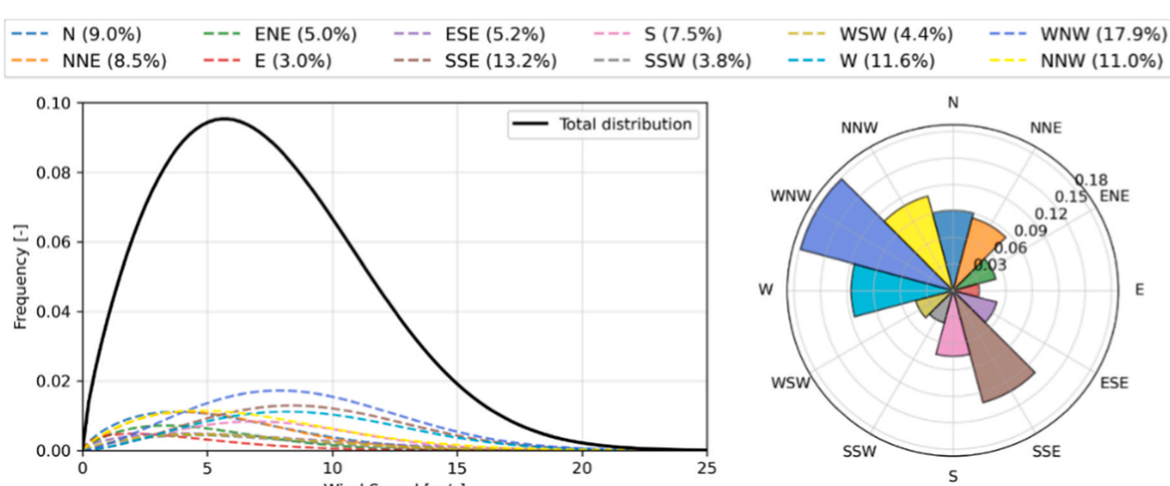

Fig. 2. Weibull distribution of wind speeds and wind rose for the selected site used for the layout optimization of the wind farms. Different colors represent different directions.

resolution of wind data was increased from 1 h to 10 min following a procedure described in detail by Travaglini et al. [22].

The variability of data measured in a nearby location with a 10-min time resolution was applied to the original 1-h resolution dataset (Figure A 2 in the Appendix). The 10-min measured values were first normalized with respect to their hourly means to extract a set of variability factors describing how each short-term point deviates from the hourly average. These factors were then applied to the ERA5 hourly series, transferring the observed intra-hour variability to the reanalysis dataset and generating a refined 10-min wind speed profile consistent with local short-term fluctuations.

Ideally, a representative multi-year period would also be derived for wind speed to ensure full consistency with the TMY used for solar energy. However, this was not feasible due to the lack of long-term high-resolution wind data required for constructing an anomaly-free representative period.

3.3. Floating photovoltaics modeling

The FPV model simulates the operation of a free-standing and open-structure monofacial module from Ref. [23]. Fig. 3 shows the scheme of the considered FPV structure: modules are mounted facing south with a 30° tilt (β) and supported by a modular raft floating structure [24] that raises their surface 1.5 m above the water (h_w) and maintains a ratio between modules' length and inter-row spacing (L/d_r) of 1.5. Like all other floating elements of the farm, the FPV floaters are attached to the seabed via catenary moorings.

The mathematical modeling of the FPV production, realized using a set of libraries from the pvlib toolbox [25], is schematized in the flowchart in Figure A 3 in the Appendix.

First, the position of the sun during the selected time frame with the desired time resolution was obtained using the function "get_solarposition" from the "location" class. Starting from the coordinates of the selected site, the function returns the apparent zenith and azimuth angles for every timestep of the analysis.

Next, the DNI, GHI, and DHI (defined as in Section 3.1), together with the apparent zenith and azimuth angles and with the surface tilt and azimuth of the panels, are passed to the "get_total_irradiance" function from the "irradiance" class of pvlib. This function determines total in-plane irradiance and its beam, sky diffuse and ground reflected components, using the specified sky diffuse irradiance model. In this analysis, the resulting Plane of Array (POA) irradiance is required for the calculation of power production from the panels.

As suggested in the pvlib documentation, the temperature variation of the panels (T_C) is then calculated using the PVSyst model according to Eq. (1). The model takes as input the POA irradiance (POA_{irr}), the air temperature (T_a), and the wind speed at 2m height (w_{2m}) and requires two heat loss coefficients, one dependent (U_v) and one independent (U_c) on the wind speed. The formula also requires an absorption coefficient (α) and a trial value of the external module efficiency (η_m). The heat loss coefficients used are also related to the free-standing and open-structure monofacial module [23] and reported in Table 2.

$$T_C = T_a + \frac{\alpha POA_{irr}(1-\eta_m)}{U_c + U_v \cdot w_{2m}} \tag{1}$$

Once the temperature variation is computed, the efficiency of the module is corrected according to Eq. (2), where γ is the temperature coefficient [29].

$$\eta = \eta_{STC}[1 - \gamma(T_C - T_{STC})] \tag{2}$$

Finally, two loss factors related to the floating operation of panels were included in the equation to consider the effect of waves and humidity.

Nysted et al. [27] developed a technique to estimate wave-induced losses (WIL) in floating PV farms resulting from changes in tilt and mismatch losses. WIL depends on the significant wave height (SWH) characterizing the site. The average SWH extrapolated from 20 years of data from ERA5 related to the installation area is 1.15m. According to Nysted et al., WIL values for sea states with SWH around 1.0 m range between 6.7 % (0°N) and 7.8 % (50°N). The case study considered here is located near the Sicilian coast, at an intermediate latitude (~38°N). Since the site experiences similar sea-state conditions, the study adopts a representative mid-range value of 7 %, consistent with the ranges reported in the reference. As no validated model on the motion interaction between wind turbine floaters and FPV exists yet, the analysis uses open-sea wave conditions to estimate WIL.

Goswami [28] studied the effect of humidity on the generation capacity of FPV and found that the performance ratio is 6.6 % lower, on average, than for land-based installations due to moisture and water ingression. Therefore, this study also considers a humidity loss (HL) in the power production equation.

The proposed FPV model does not specifically include other sources of power loss mechanisms, such as the potential impact of dust and fouling from birds. While these mechanisms may influence the power output of modules, they are highly site dependent and require dedicated analyses to reflect the specific mitigation strategies that should be adopted in each case.

Table 2
Main assumptions for FPV modeling.

Parameter	assumption	Reference
η_{STC}	16.5 %	[23]
P_{spec}	162.3 W/m^2	[23]
γ	0.004	[26]
T_{STC}	25 °C	
U_c	31.9 W/m^{2}K	[23]
U_v	1.5 W/m^{3}Ks	[23]
WIL	7 %	[27]
HL	6.6 %	[28]

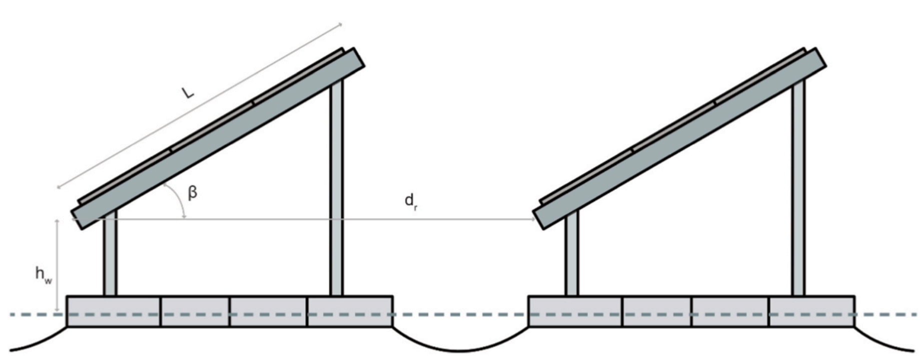

Fig. 3. Schematic of the geometrical dimensions considered in the positioning of subsequent platforms of floating PV panels. Horizontal dashed line represents the average water level.

The power production (P) from the PV field can then be calculated as in Eq. (3), given the area of the PV modules (A).

$$P = \eta \cdot A \cdot POA_{irr} \cdot (1 - WIL) \cdot (1 - HL) \tag{3}$$

Table 2 summarizes the main assumptions behind FPV modeling.

3.4. Floating wind farm modeling

The wind farm model simulates the power production coming from a wind farm composed of a variable number of 15 MW IEA floating offshore wind turbines [30], assuming a semi-submersible platform as a floater. Each wind turbine has a nominal power output of 15 MW, a cut-in speed of 3 m/s, a rated speed of 10.6 m/s and a cut-out speed of 25 m/s.

Fig. 4 shows the flowchart of the mathematical model used to optimize the wind farm layout and the subsequent PyWake simulation to obtain the time-dependent power production. First, the TOPFARM package developed by DTU Wind Energy [31] was used to optimize the layout of the wind turbines in the available sea lot as proposed by some of the authors in Ref. [32]. Then, a time-dependent simulation using the PyWake tool is performed to obtain the time-varying power production from the optimized wind farm layout. Table 3 summarizes the main assumptions made for the wind farm layout optimization.

The layout optimization takes as input the boundaries of the available sea lot and the initial positioning of the wind turbines (Figure A 4 in the Appendix). The initial positioning assumes that the wind turbines are homogeneously distributed within the available area, leaving a central free space reserved for the electrical substation.

In each iteration, TOPFARM tests a new WF layout, starting with estimating the power production of the wind farm. To this end, the wind energy distribution, divided into the twelve directions, is taken as input by the model for the power calculations. These Weibull distributions (Fig. 2) are combined with the power curve of wind turbines for the evaluation of the Annual Energy Production (AEP) of the farm, adopting the Niels Otto Jensen (NOJ) model [33] to compute the wake deficit caused by wind turbines, considering an expansion factor of 0.04.

To take into account the different height between the data source and the hub heights (150 m), a power-law has been adopted for the extrapolation of the wind speeds, assuming 0.1 as the shear exponent, according to the best practice for offshore installations [34]. Per each iteration, the inter-array cable layout is optimized by minimizing total cable length while keeping WT locations fixed. Afterward, CAPEX and OPEX are finally estimated to find the objective function.

The goal of the optimization is the minimization of the final LCOE of the farm, which requires a set of economic assumptions related to the wind farm (described in Section 3.6). The optimal LCOE comes from the trade-off between a higher distance between the turbines, which minimizes wake losses and hence increases the AEP, and a tighter positioning, which minimizes the cable length and thus decreases investment costs. The minimum distance at which the turbines can be placed is equal to four times the turbine diameter [35]. To drive economic optimization, TOPFARM requires as input also the costs of all the components involved.

Table 3
Main assumptions for the wind farm layout optimization.

Parameter	Assumption
Hub height	150m
Rotor diameter (D_R)	242m
Platform	Semisubmersible
Sea lot dimension	32x14 km
Water depth	390 m
Minimum distance	4 D_R
Distance from shore	60 km
Wake model	NOJ
Optimizer	COBYLA
Tolerance	10^{-8}
Max iter	10^6

The selected optimization driver was the Constrained Optimization BY Linear Approximation (COBYLA), a Gradient-Free Optimization Algorithm from SciPy. The optimizer is constrained by a maximum of 10^6 iterations and has a tolerance of 10^{-8}.

The layouts obtained by following the proposed approach represent a theoretical optimum. Practical constraints related to access, maintenance, safety, and installation remain strongly dependent on the specific site and developer and were not explicitly modeled. Indeed, their inclusion would require detailed, location-specific analyses to be treated appropriately.

After the optimization of the layout, a time-dependent simulation of the power production from the wind farm is performed using the PyWake wind farm simulation tool [33]. The time-dependent simulation uses the same wake model and power curve used for the layout optimization but takes as input the wind speed and wind direction time series described in Section 3.2 instead of the statistical distributions.

To analyze the first hybrid scenario, this process was repeated multiple times to optimize sixty-seven wind farms comprising an increasing number of wind turbines and cover the whole power share span that wind energy can cover in the solar-wind hybrid system.

3.5. Hybrid system modeling

The total power production from the hybrid farm is computed as the sum of the export from the wind turbines ($E_{export,FWT}$) and from the floating PV panels ($E_{export,FPV}$), considering the rated capacity of the export cable.

The solar production trend is calculated during the typical meteorological year, while the wind production is computed across two years of operation. Power production from the hybrid system is then obtained by adding the 1-year solar production to both the wind production years. The mean yearly performance of the overall system is then computed as the average of the two.

In the first scenario, the study considers the installation of a hybrid system characterized by a total rated power of 1 GW. To cover the whole power range, sixty-seven configurations involving an increasing number of 15 MW wind turbines are considered, while the solar installation is tailored to reach the total target size. All the energy produced by the hybrid farm can be exported to the shore by the 1 GW export cable.

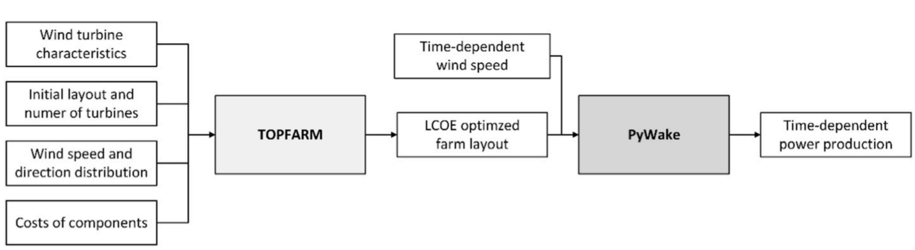

Fig. 4. Flowchart of the mathematical model used to optimize the wind farm layout and the subsequent PyWake simulation to obtain time-dependent power production.

In the second scenario, the study considers the introduction of FPV to a 1 GW wind farm already equipped with a 1 GW export cable. In this case, system modeling considers that the export cable may act as a bottleneck. When solar panels produce during hours of low wind, the solar production increases the overall export of the system. However, when solar and wind production are simultaneous, the total export may be higher than the transmission capacity of the export cable. In those moments, wind energy has the dispatch priority because of the higher remuneration, while solar energy can be curtailed.

The Capacity Factor (CF) of the hybrid system is calculated as the ratio between the total exported energy and the nominal energy production (as in Eq. (4)).

$$CF = \frac{E_{export,FWT} + E_{export,FPV}}{E_{nominal,FWT} + E_{nominal,FPV}} \tag{4}$$

The Utilization Factor (UF) of the cable is instead calculated as the ratio between the total exported energy and the maximum energy export of the cable (as in Eq. (5)). For a configuration with a total rated power of 1 GW, the CF of the system and the UF of the cable are equal.

$$UF = \frac{E_{export,FWT} + E_{export,FPV}}{E_{nominal,cable}} \tag{5}$$

3.6. Economic assumptions

The main economic metric used to evaluate the economic convenience of system configurations is the Net Present Value, computed as in Eq. (6). The NPV calculation considers the different remuneration for the wind farm (R_{FWT}) and for the PV field (R_{FPV}). In the present case study, only the energy that the farm manages to transport to the shore and to inject into the grid (E_{export}) is rewarded.

The calculation considers a lifetime (n) of the system of 30 years, and a discount rate (i) of 7 %. The capital expenditure (CAPEX) indicates the total investment cost incurred to build the entire system. Earnings come from the total revenues minus the operating expenditure (OPEX) associated with the maintenance of the system. The yearly OPEX is computed as a percentage of the initial investment (5 %).

$$NPV = \sum_{t=1}^{n} \frac{\left(E_{export,FWT} \cdot R_{FWT} + E_{export,FPV} \cdot R_{FPV} - OPEX\right)_t}{(1+i)^t} - CAPEX \tag{6}$$

Results also report the year in which the NPV becomes positive, and the investment is recovered, i.e., the Payback Period (PBT).

The LCOE of the hybrid system can be calculated following the standard approach, except for considering only the energy exported at the denominator (Eq. (7)).

$$LCOE = \frac{\sum_{t=1}^{n} \frac{(CAPEX_t + OPEX_t)}{(1+i)^t}}{\sum_{t=1}^{n} \frac{\left(E_{export,FWT} + E_{export,FPV}\right)_t}{(1+i)^t}} \tag{7}$$

Table 4 summarizes the main techno-economic assumptions and the cost of components breakdown made for the calculation of the NPV and LCOE. The investment costs related to the overall floating structure, wind turbines, the electrical substation, the project, and installation were calculated using the FWT cost model proposed by some of the authors in Ref. [32], taking as input the distance from shore, the project duration, the discount rate, and the export cables cost.

Few cost references are available in the literature for the installation of FPV on the open sea. The prices reported by different projects are distributed in a wide range. According to Nebuloni et al. [23], the cost of FPV is 25–30 % higher than ground-mounted photovoltaics (GPV). This study considers four prices: a low price baseline (+25 % of the base price for GPV), a slightly higher baseline (+30 % GPV), an average price from the literature ([39]) and a higher CAPEX reported in a recent position paper by AERO [42].

The present analysis focuses on the operational techno-economic performance of the hybrid floating system and does not include other aspects such as decommissioning. Further developments could involve a comprehensive evaluation of the decommissioning phase, involving detailed site-specific information, logistics, and scenario-based assessments based on recent contributions in the field of offshore projects [43].

Table 4
Main techno-economic assumptions.

Component	assumption	Reference
Intra-array cables	750 €/m	[36]
Export cable	2.7 M€/km	[36]
Electrical substation	324 €/kW	[37]
Installation costs	~300 €/kW	[37]
Project costs	700 €/kW	[37]
Discount rate (i)	7 %	
Lifetime of project (n)	30 years	
Sea lot dimension	32x14 km	
Distance from shore	60 km	
Water depth	390 m	
FWT energy remuneration (R_{FWT})	185 €/MWh	[38]
FPV energy remuneration (R_{FPV})	105 €/MWh	[38]
FWT cost	FWT cost model	[32]
FPV cost	low (+25 % GPV) - 0.91 M€/MW	[39,40]
	low (+30 % GPV) - 1.04 M€/MW	[39]
	average - 1.3 M€/MW	[39,41]
	high - 1.5 M€/MW	[42]

4. Results and discussion

4.1. Wind layout optimization

Sixty-seven layout optimizations were conducted to obtain the best spatial arrangement of an increasing number of wind turbines to analyze the first hybrid scenario, where different hybrid farms with varying shares of wind and solar energy to reach the 1 GW nominal output are considered. Table A in the Appendix reports the main results from the optimization of the sixty-seven layouts comprising an increasing number of 15 MW wind turbines in terms of AEP, CF, and wake losses.

The TOPFARM optimization framework finds the layout that minimizes the LCOE by looking for the best tradeoff between the minimization of intra-array cable length and AEP maximization (i.e., wake losses minimization). However, due to the increasing wake interaction between turbines when the density of wind turbines in the available sea lot increases, the wake losses inevitably increase, and the CF of the farms gradually decreases with the number of WTs. As a result, the AEP is not linearly dependent on the number of WTs installed.

Fig. 5 shows four examples of wind farm layout optimization considering a) ten turbines, b) thirty-four turbines, c) fifty-four turbines, and d) sixty turbines. The purple dashed lines represent the spatial limitation corresponding to the 14 × 32 km available sea lot. With a limited number of wind turbines (Fig. 5 (a)), the optimizer aligns them on a row perpendicular to the predominant wind direction. This solution allows for minimizing the cable length even in layouts without strong interactions between rows (Fig. 5 (b)).

With a high number of turbines (Fig. 5(c) and (d)), the impact of wake losses on the AEP increases, and the optimizer starts pushing the WTs to the boundaries of the available space, at the expense of longer intra-array cable lengths.

Fig. 6 displays the result of the topological optimization of a 1 GW Wind Farm composed of sixty-seven 15 MW IEA wind turbines. Grey dots represent the initial position that the optimizer considers, while the light blue dots represent the optimal positioning for the minimization of the LCOE. The yellow square represents a 600-MW FPV array for size comparisons, occupying an area of 3.7 km^2 (1.92 × 1.92 km square). FPV modules are going to be installed in the center of the wind farm, in proximity to the electrical substation.

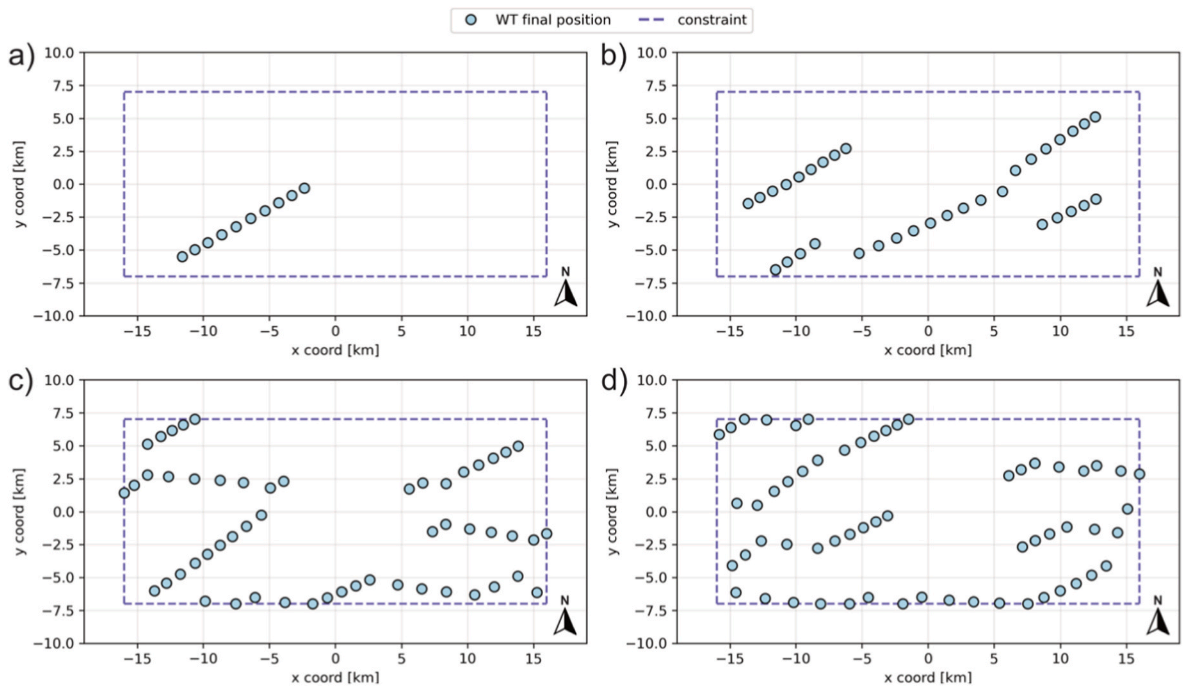

Fig. 5. Four examples of wind farm layout optimization considering a) ten turbines, b) thirty-four turbines, c) fifty-four turbines, and d) sixty turbines.

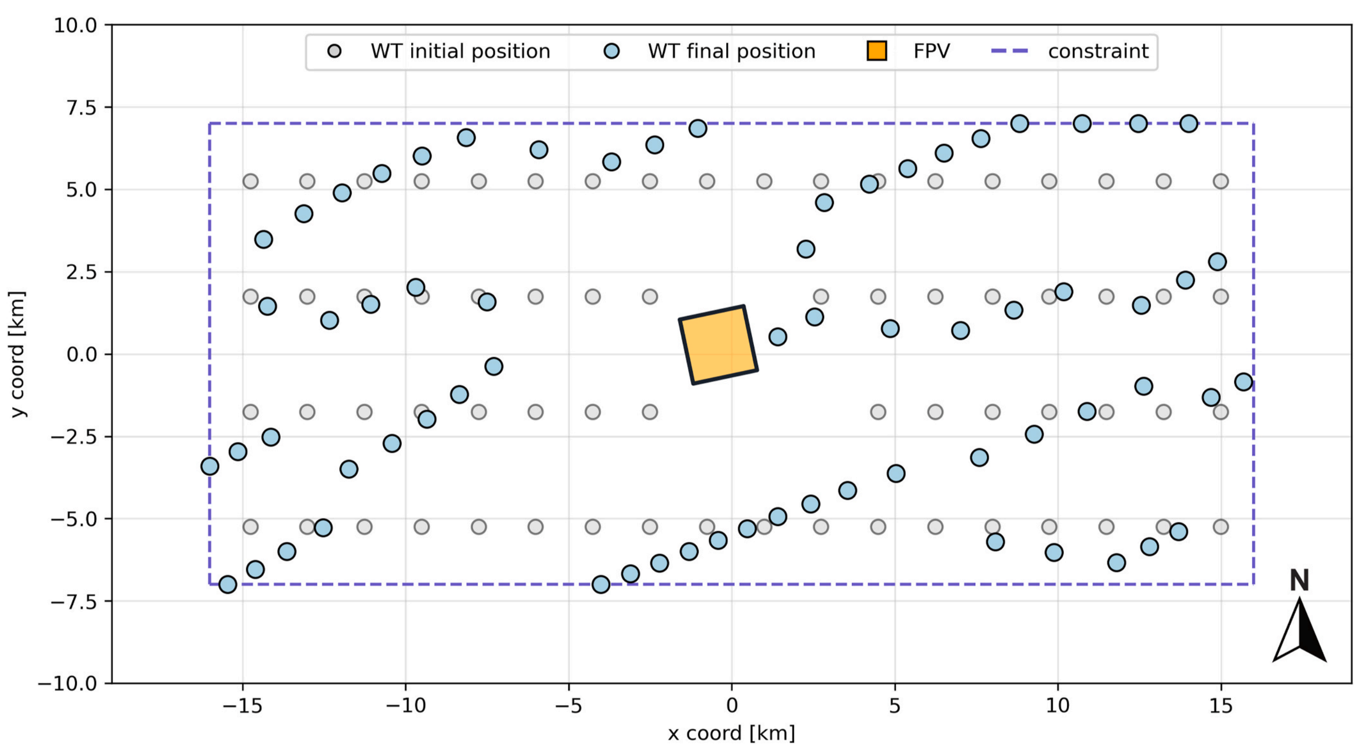

Fig. 6. Optimized layout of the 1 GW wind farm (blue dots) and comparison with initial positioning of wind turbines (grey dots) and area occupied by the PV array (yellow square).

4.1.1. 1 GW wind-only farm

The optimized layouts, together with the two years of wind speed data with a 10-min time resolution, were the inputs for the time-dependent analysis using PyWake. For all sixty-seven optimized layouts, the trend of power output from the wind farms was obtained to analyze the matching degree with the solar production in the second hybrid scenario, when additional solar power is added to a 1 GW wind farm, maintaining the 1 GW export cable.

Fig. 7 shows the trend of the 10-min power output and the daily energy production from a 1 GW wind farm over a year of operation. Table 5 reports the main techno-economic outcome from the analysis of a 1 GW wind farm in terms of AEP, CF, LCOE, capital expenditure, and NPV.

Since the time-dependent analysis uses a different input (two-year

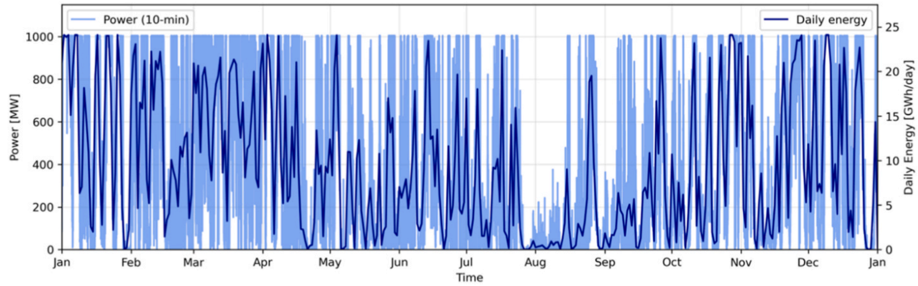

Fig. 7. Trend of the power output and the daily energy production from a 1 GW wind farm during a year of operation.

Table 5
Techno-economic outcome of the 1 GW wind farm with optimal layout.

AEP [GWh/y]	CF [%]	LCOE [€/MWh]	I_0 [B€]	NPV [M€]	PBT [y]
3665	41.6	137.6	3.84	2132	12

wind speed trend in Figure A 2) than the statistical analysis (Weibull from 10 years of data in Fig. 2), the results are slightly different than what was reported in Table A for the 1 GW wind configuration.

In this wind-only scenario, the CF is 41.6 % and the plant produces 3.67 TWh/y. The LCOE is 137.6 €/MWh, and the energy is remunerated, according to FER2, at 185 €/MWh. As a result, the NPV after 30 years of operation is 2.13 B€.

4.2. Floating PV production

The typical meteorological year from NSRDB containing GHI, DNI, DHI (Figure A 1) and wind speed and ambient temperature were the inputs to the FPV model (Figure A 3).

Fig. 8 shows the resulting trends over two weeks of operation. Fig. 8 (a) shows the resulting POA global irradiance resulting from the application of the total irradiance function. Considering the heating effect

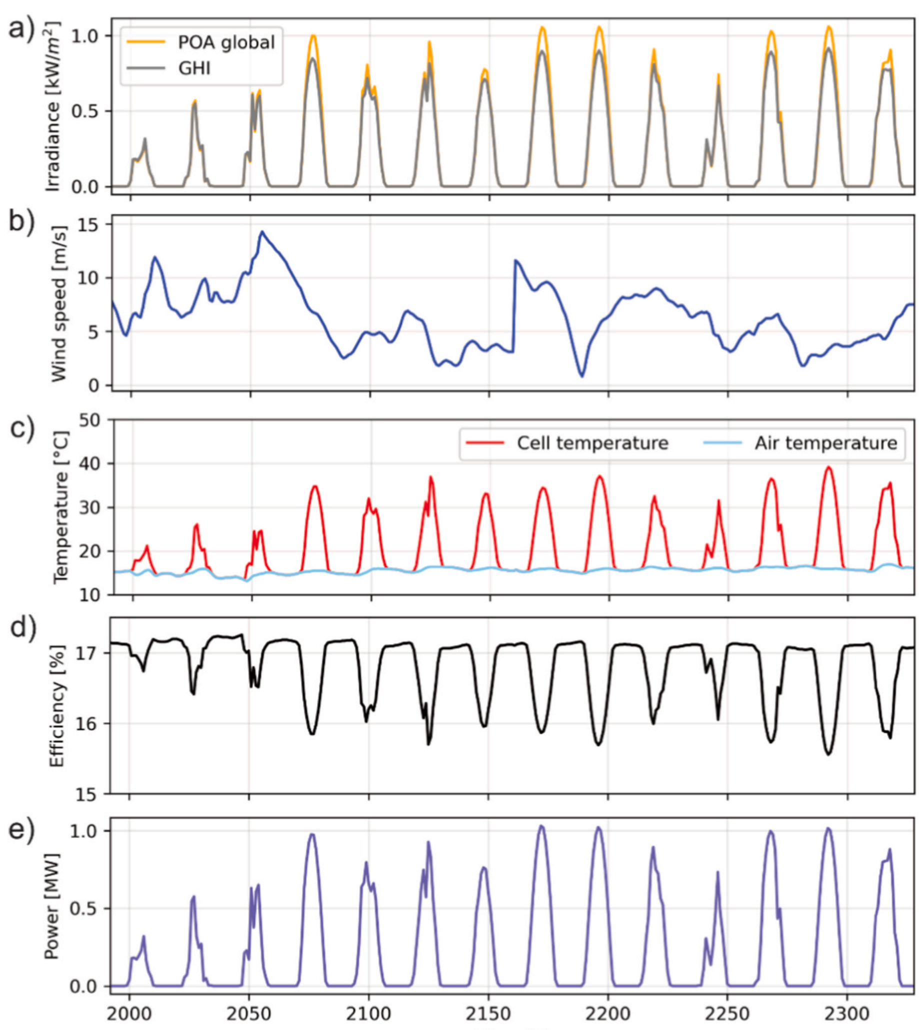

Fig. 8. Time trend of a) GHI and POA global irradiance, b) wind speed at 2m height, c) cell and air temperature, d) efficiency, and e) power production from a 1 MW rated PV field.

from solar irradiance in Fig. 8 (a) and the cooling effect of wind speed in Fig. 8 (b), the thermal model outputs the cell temperature (red line) in Fig. 8 (c), where it is compared with air temperature (light-blue line). The efficiency variation in Fig. 8 (d) has a trend opposite to the temperature variation. The trend in power production in Fig. 8 (e) is strongly linked to solar irradiance but scaled according to the efficiency variation, wave-induced losses, and humidity losses.

4.2.1. 1 GW FPV only farm

Fig. 9 shows the trend of the power output and the daily energy production from a 1 GW solar farm during the whole typical year. Table 6 reports the main techno-economic outcome from the analysis of a 1 GW solar farm in terms of AEP, CF, LCOE and NPV. The reported installation cost I_0 considers the whole installation of the floating system, also comprising the 1 GW export cable.

In this solar-only case, the CF of the system is 18.1 % and the plant produces 1.59 TWh/y. Considering the lowest FPV price of 0.91 M€/MW, the LCOE of the solar-only option is 88.8 €/MWh, and the NPV after 30 years is 317 M€. If higher prices are considered (1.04 M€/MW), the LCOE of the solar-only farm becomes 99.6 €/MWh, very close to the remuneration of the FPV. Consequently, the NPV of the system drops considerably to 106 M€.

When average (1.3 M€/MW) or high (1.5 M€/MW) prices are considered, the LCOE becomes 121.1 and 137.7 €/MWh, respectively. Consequently, in these price scenarios, the NPV of solar-only farms is negative, indicating that the remuneration proposed by the FER2 would be unsustainable if companies are going to face installation costs equal to or higher than the ones reported by AERO [42].

Fig. 10 shows the results from a sensitivity analysis on LCOE and NPV varying FPV price, with comparison with the remuneration set by FER2. The analysis revealed that the threshold price that makes the LCOE of FPV higher than the remuneration (105 €/MWh) is equal to 1.11 M€/MW. As a consequence, if an FPV project has to sustain an installation cost higher than this threshold, the NPV cannot be positive according to the remuneration proposed by FER2.

4.3. Hybrid scenario 1: 1 GW hybrid farm

The first hybrid scenario considers a floating system combining wind turbines with floating PV panels to reach a total nominal power output of 1 GW. The sixty-seven layouts of wind farms comprising a number of wind turbines from one to sixty-seven were optimized according to Section 3.4 and then paired with floating PV arrays to reach the target output.

Fig. 11 shows the variation of NPV, LCOE, and CF of the 1 GW hybrid system varying the wind installed power. At the left extreme of the x-axis, the plot shows the solar-only scenario described in Section 4.2.1, while at the right extreme, it shows the wind-only scenario of Section 4.1.1. Between the two extremes, the plot shows how hybrid farms perform by varying the variable shares of the two technologies.

With FPV prices lower than 1.3 M€/MW, the increase of wind power in the mix only leads to a higher LCOE, and it provides a benefit only

Table 6
Techno-economic outcome of the 1 GW floating solar farm.

FPV cost [M€/MW]	AEP [GWh]	CF [%]	I_0 [B€]	LCOE [€/MWh]	NPV [M€]	PBT [y]
0.91	1594	18.1	1.08	88.8	317	17
1.04	1594	18.1	1.21	99.6	106	24
1.3	1594	18.1	1.47	121.1	−316	–
1.5	1594	18.1	1.67	137.7	−640	–

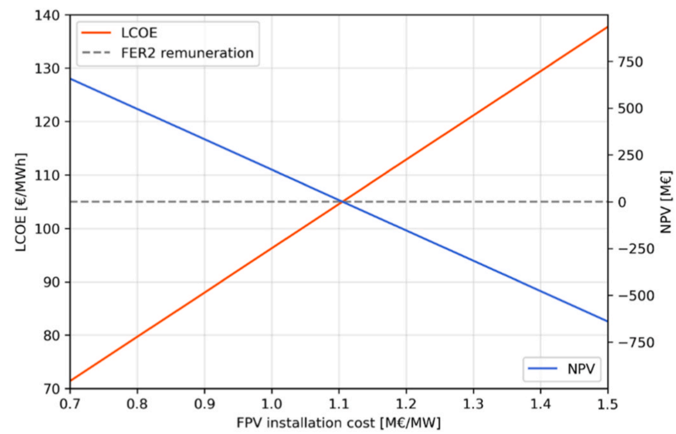

Fig. 10. LCOE and NPV sensitivity analysis on FPV price with comparison with the remuneration set by FER2.

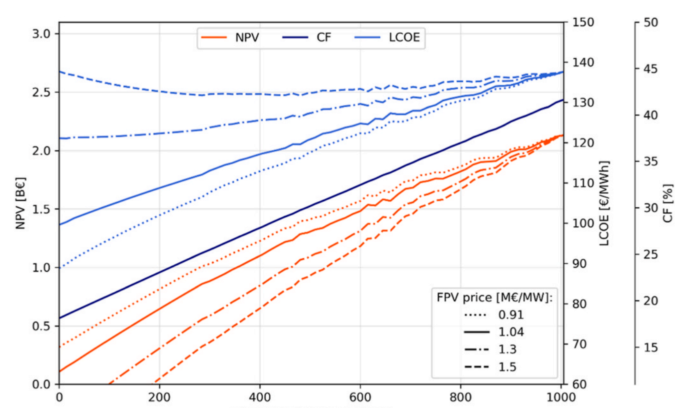

Fig. 11. Variation of NPV, LCOE, and CF of the 1 GW hybrid system varying the wind installed power.

when considering FPV prices of 1.5 M€/MW.

Considering the electricity market conditions, in the FER2 remuneration scheme (105€/MWh for FPV and 185 €/MWh for FWT) specifically, the introduction of wind energy in the mix always results in an

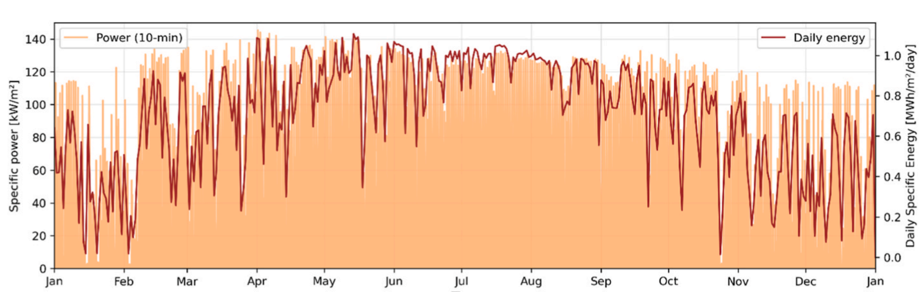

Fig. 9. Trend of the power output and the daily energy production from a 1 GW solar farm during a year of operation.

enhanced NPV (red lines in Fig. 11). In that case, the most convenient strategy is to maximize the share of wind energy in the mix due to the more convenient ratio between cost and price of wind energy compared to solar energy.

To generalize beyond the FER2 remuneration scheme, Fig. 12 shows the results from a sensitivity analysis made varying both the remuneration applied to FWT and FPV in the range between 105 and 185 €/MWh. Table 7 reports a detailed techno-economic outcome from optimal wind-solar combinations in six remuneration scenarios. For the analysis, medium prices (1.04 M€/MW) for the installation of FPV were considered, an assumption that makes the LCOE of solar energy equal to 99.6 €/MWh in solar-only configurations (Table 6). The wind-only option has, instead, an LCOE of 137.6 €/MWh (Table 5), higher than the lower part of FWT remunerations considered in the analysis.

Fig. 12 (a) shows the NPV of the optimal hybrid configuration for each possible combination of FWT and FPV remunerations. In this scenario exists a combination of solar and wind that leads to a positive NPV. Due to the lower LCOE of solar energy than wind energy, an increase in FPV remuneration makes the NPV grow at a faster rate than an increase in FWT remuneration. On the other hand, the highest values of NPV that the system can reach are possible only with high remuneration of wind energy, due to the higher AEP of WTs than PV modules.

Fig. 12 (b) shows the optimal PV power to be installed to reach the maximum NPV shown in Fig. 12 (a). The plot shows that small shares of wind in the energy mix become convenient even when the remuneration applied to wind energy is lower than the LCOE found for the wind-only option, reflecting the higher productivity and the synergy between the two sources. In hybrid systems with low wind shares, the installation cost of the export cable has a lower impact on the wind turbines, making the installation of a limited number of WTs convenient even with a lower remuneration applied to wind energy. Even if the remuneration applied to wind energy is 130 €/MWh, when the FPV still receives only 105 €/MWh, the optimal configuration involves 225 MW of wind energy.

When the remuneration applied to FWT is equal to the one applied to FPV, the system always benefits from a share of solar energy in the mix, again due to the lower LCOE of solar energy. When a medium remuneration is applied to both sources (145 €/MWh), the optimal configuration involves 840 MW of solar energy and reaches an NPV of 0.9 B€.

Table 7
Techno-economic outcome from six possible remuneration scenarios for FPV and FWT in the first scenario.

FPV rem. [€/MWh]	FWT rem. [€/MWh]	NPV [B€]	PBT [y]	PV power [MW]	WT power [MW]
105	185	2.13	12	0	1005
125	165	1.24	16	15	990
145	145	0.9	12	840	165
165	165	1.46	12	525	480
185	185	2.17	11	285	720
105	130	0.14	24	780	225

The higher CF of wind energy makes this convenience decrease with the increase of FWT remuneration: if both sources receive 165 €/MWh, the optimal PV power decreases to 525 MW.

The plot also shows that, when the wind energy has a remuneration of 185 €/MWh (as expected by the FER2), solar energy must be remunerated similarly to be convenient in the mix. When both sources receive the maximum remuneration, the optimal configuration comprises 285 MW of PV and reaches an NPV of 2.17 B€.

4.4. Hybrid scenario 2: 1 GW wind farm and variable PV generation

4.4.1. Complementarity between wind production and additional solar power

The second scenario considers adding a variable solar production capacity to a 1 GW offshore floating wind farm, connected to shore by a 1 GW export cable. This time, the energy remunerated less (solar power in the FER2 scenario) exceeding the cable capacity is curtailed.

Fig. 13 shows an example of power flows from the 1 GW floating wind farm (grey line) and additional 600 MW solar generators (orange line) in the second scenario. The red line represents the constraint from the 1 GW export cable, which forces the system to curtail energy export when production exceeds the transmission capacity. The green areas represent the allowed energy export, given by the sum of wind and solar energy when the total generation is lower than 1 GW, while orange areas represent the curtailed energy, i.e., the solar generation that exceeds the maximum output.

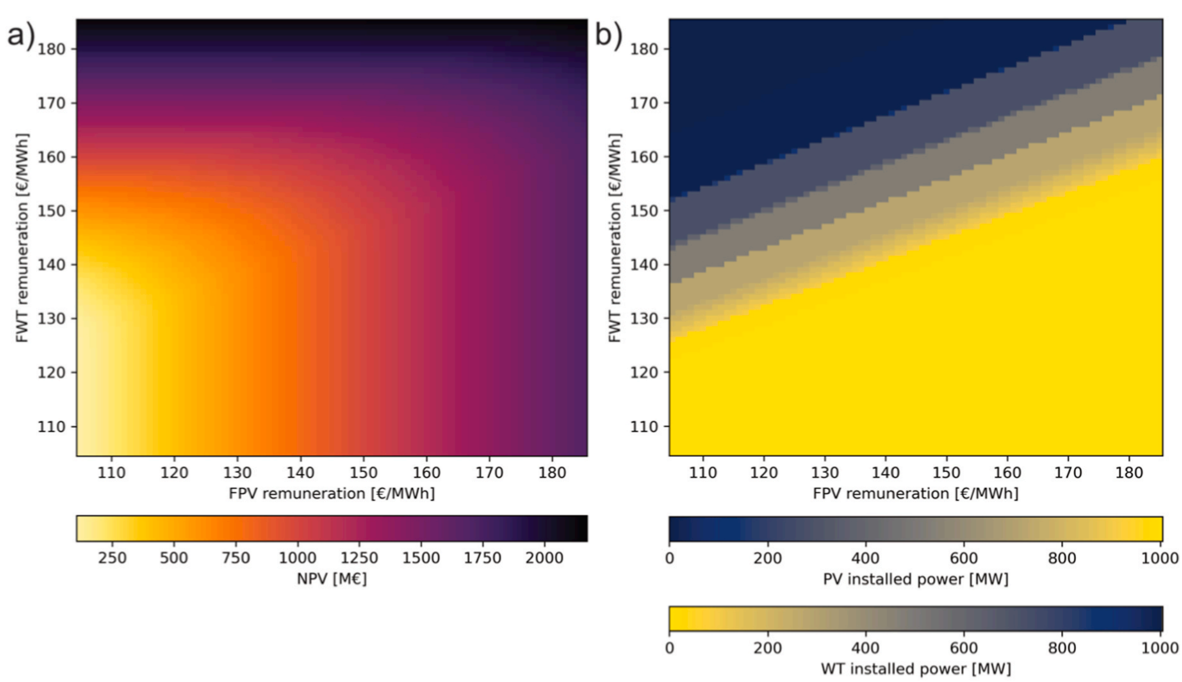

Fig. 12. Sensitivity analysis on the variation of the remuneration applied to floating wind energy and floating solar energy and resulting a) NPV and b) optimal PV power to be installed in the first hybrid scenario.

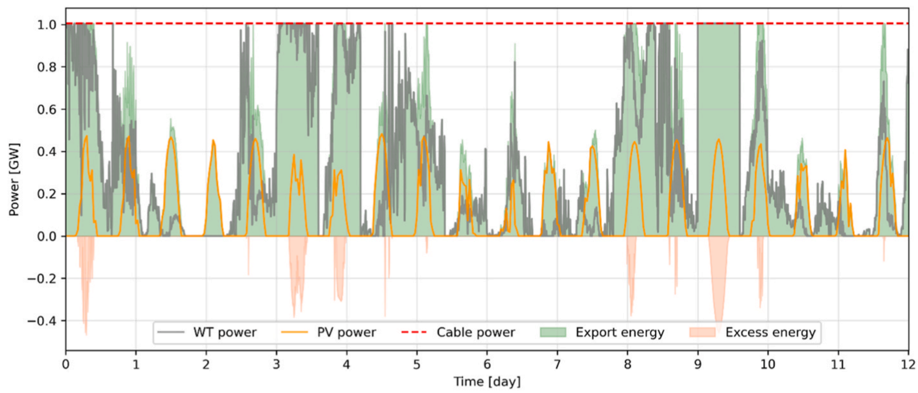

Fig. 13. Power flows from WT and PV, constrained by the rated power of the export cable and resulting in export and excess energy.

Wind turbines are prone to produce less during summer (Fig. 7), while the PV field shows the opposite trend (Fig. 9). Figure A 5 in the Appendix compares the daily energy production from a 1 GW wind farm (grey line) and a 600 MW FPV field (orange line) and shows the curtailed energy when the systems are sharing the same 1 GW export cable (red line). The minimum power curtailment happens indeed during summer and winter, where the trend is opposite: in summer solar production peaks while wind production is lower, whereas in winter wind production peaks while solar production drops. The maximum curtailments happen instead during spring and autumn. Overall, the two sources show a good matching degree, and, even in this case, the annual energy that must be curtailed is only 23.6 % of the solar production where the nominal solar power is 60 % of the wind power.

The temporal complementarity between wind and solar resources found for the Sicilian site aligns with patterns reported for the western Mediterranean in Vázquez et al. [4]. Their analysis shows that in the Spanish Mediterranean zones the wind resource peaks in winter, while PV potential is maximised in summer, with frequent droughts for solar during night-time.

Fig. 14 shows the variation of the AEP export, percentage of curtailed PV production, and capacity factor of the hybrid system with the introduction of PV installed power.

The AEP sharply increases at the beginning, while the percentage of solar energy that is curtailed grows at a slow rate. This result highlights a complementarity degree between solar and wind energy: PV panels produce when wind turbines are not working at their maximum potential, allowing for a steadier and more frequent energy export to the shore. Nonetheless, the overall CF of the system decreases, since solar energy is characterized by a lower CF than wind turbines.

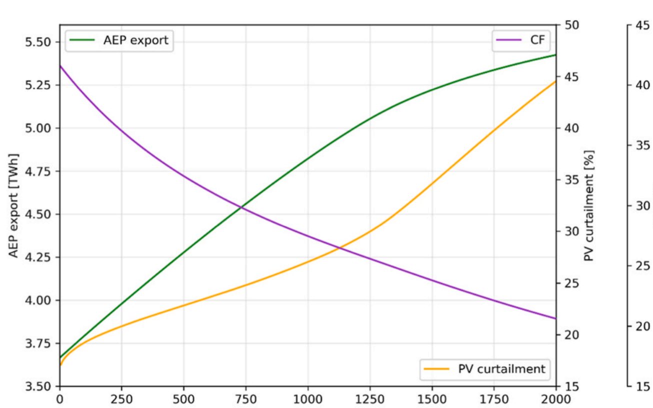

Fig. 14. Variation of annual energy export, percentage of curtailed PV production, and capacity factor of the hybrid system with the introduction of PV installed power.

At a PV installed power of around 1250 MW, the export cable starts acting as a bottleneck, and PV curtailment reaches 30 %. The share of PV energy that cannot be exported to shore starts rising more rapidly (up to 45 % with 2 GW PV added), and the total energy export starts saturating. The rise in PV curtailment has a direct impact on the overall economic return of the investment, as shown by the NPV and LCOE trend and described as follows.

The higher wind capacity factor in the Sicilian case study is also in line with results from Yuan et al. [3], showing that in nearshore marine regions of East Asia the optimal wind share in the mix is between 50 and 80 %.

Results from this scenario can be compared with the assessment presented by Delbeke et al. [18], who added FPV capacities between 0.5 and 3.5 GWp to a 2262 MW offshore wind farm, sharing the same export cable of 2254.4 MW. FPV sizes correspond additional solar shares between about 22 % and 155 % of the wind capacity, with an optimal sizing of 3020 MWp (133 % of wind). Under their conditions, the fraction of curtailed PV electricity reaches 16 % at the selected trade-off point, while the transmission capacity factor rises from 37.1 % in the wind-only case to 50 % with FPV. In the present study, FPV capacity is varied up to about 1250 MW, i.e., 125 % of the 1 GW wind farm. The utilization of the export cable increases from 41.6 % to 56.2 % and then saturates, but the export constraint becomes limiting at lower PV shares. When FPV reaches 60 % of the wind capacity (600 MW), the annual curtailed solar energy arrives at 23.6 %, a level that Delbeke et al. [18] only approach for much higher PV-to-wind ratios. These differences indicate that, while the qualitative benefits of cable pooling are robust across sites, the PV share that maximizes those benefits is location-specific and more constrained in the Sicilian case due to the stronger bottleneck of the 1 GW export cable.

By considering a specific case study together with an actual remuneration scheme, this paper goes beyond technical assessments and shows how such hybrid systems would perform in an actual market.

4.4.2. *Economic convenience of cable pooling*

Fig. 15 shows the variation of NPV, LCOE, and UF of the cable with the introduction of PV installed power. Even if the CF of the system decreases with the introduction of solar energy (Fig. 14), the UF of the 1 GW cable increases with the installation of solar energy.

When considering high-industry prices (1.5 M€/MW - dashed lines) or average prices (1.3 M€/MW – dash-dotted lines), the introduction of even small amounts of solar generation worsens all the economic metrics of the hybrid system. When the LCOE of FPV is higher than the remuneration proposed by FER2, the system benefits from the installation of solar capacity only from a technical point of view (higher exploitation of the export cable).

When considering very low FPV prices (0.91 M€/MW - dotted lines), the introduction of additional solar capacity has a beneficial effect both from the LCOE and the NPV point of view. The LCOE, calculated

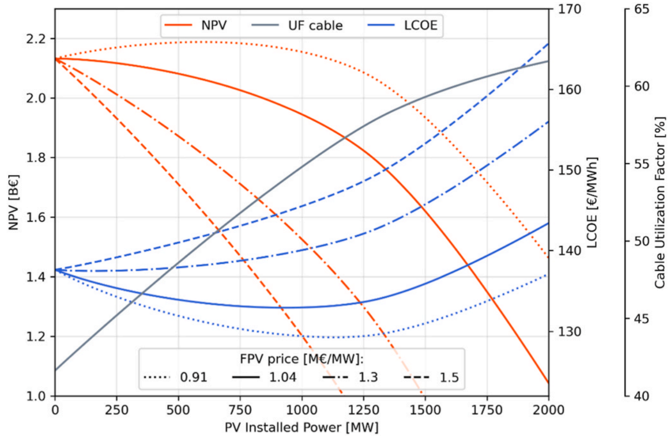

Fig. 15. Variation of NPV, LCOE, and utilization factor of the cable with the introduction of PV installed power.

considering only the energy that the hybrid farm can export to shore via the 1-GW cable, decreases with the introduction of cheap solar energy. The LCOE trend presents a minimum (129 €/MWh) at a PV capacity of 1130 MW, almost doubling the wind installed power. This point is localized close to the PV power at which the exported energy starts saturating, i.e., around 1250 MW, as shown by the flattening of the UF curve. With the introduction of a solar capacity of this magnitude, the UF of the cable rises from 41.6 % to 56.2 %. After that, the amount of solar energy that must be curtailed starts rising sharply, and the installation of more PV capacity starts being inconvenient.

At the same time, an increase in revenues takes place due to the higher energy production and improved use of the export cable. The NPV trend also shows a quick drop when the cable starts acting as a bottleneck. However, the maximum NPV (2.19 B€) is localized at a lower solar capacity (595 MW) than the one that minimizes the LCOE. The different remuneration and thus the lower margin of profit of solar energy create this difference.

When considering slightly lower FPV prices (1.04 M€/MW – solid lines), the introduction of additional solar power still has a beneficial effect on the LCOE, whose minimum (132.9 €/MWh) is now characterized by a configuration involving 930 MW of PV. On the other hand, the much lower gap between the cost of producing solar power and the remuneration applied to it makes the optimal NPV of the configuration shift to a solution combining the 1 GW wind farm with only 10 MW of installed FPV.

As for the first scenario, a sensitivity analysis on the remuneration applied to wind and solar floating power in the second hybrid scenario (Fig. 16) allows for generalizing beyond what is proposed by FER2, again considering a medium FPV price of 1.04 M€/MW (LCOE of 99.6 €/MWh, Table 6). In this hybrid scenario, extra energy must be curtailed when the total generation of the system exceeds the transmission capacity of the export cable, fixed at 1 GW. Energy curtailment is applied to the source that is remunerated less from the electrical market: solar energy in the upper-left part of the plots and wind energy in the lower-right part.

Fig. 16 (a) shows the NPV of the optimal combination of 1 GW wind power and extra solar power. Fig. 16 (b) shows that the optimal additional solar power only varies with the remuneration applied to FPV. This time, as the installed wind power is always equal to 1 GW, the NPV in situations when the remuneration applied to wind energy is low is inevitably negative. When the extra PV power is zero, the remuneration of FWT must be at least equal to the LCOE of wind-only options (137.6 €/MWh, Table 5). In those cases, a higher remuneration of solar energy makes it possible to recover the investment, and the negative NPV front in Fig. 16 (a) shows a decreasing trend with the FPV remuneration.

Table 8 reports the detailed techno-economic outcome from five

Table 8
Techno-economic outcome from five possible remuneration scenarios for FPV and FWT in the second scenario.

FPV rem. [€/MWh]	FWT rem. [€/MWh]	NPV [B€]	PBT [y]	PV power [MW]	WT power [MW]
105	185	2.13	12	0	1005
125	165	2.25	17	800	1005
145	145	0.7	20	1100	1005
165	165	1.94	14	1200	1005
185	185	3.19	11	1300	1005

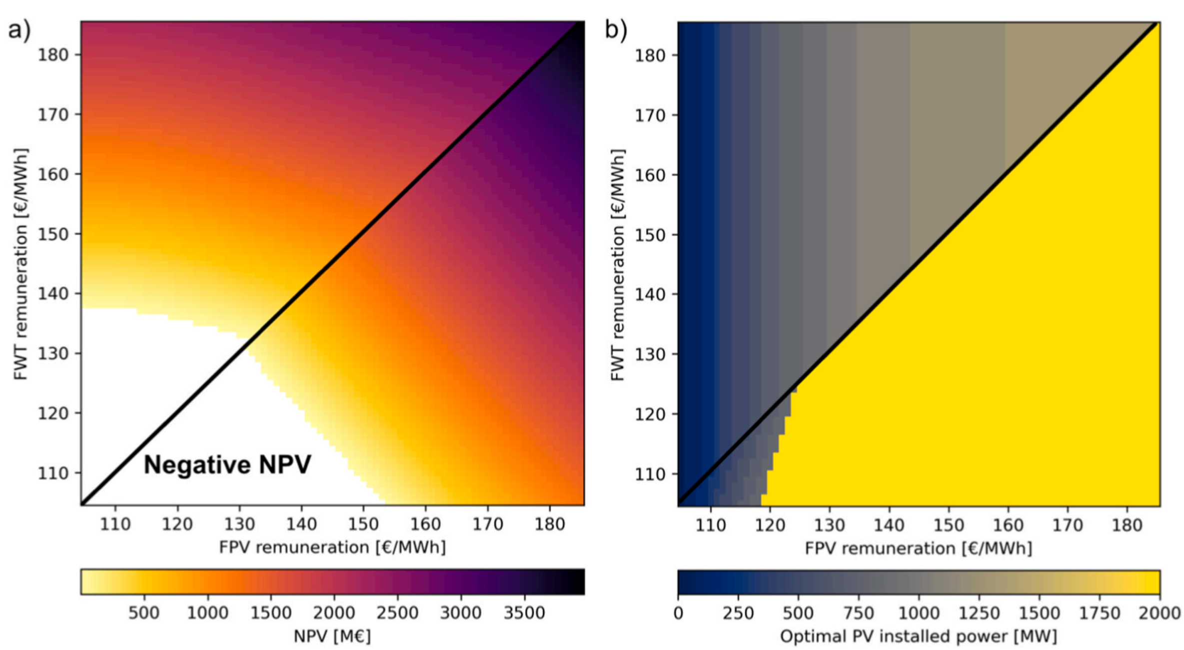

Fig. 16. Sensitivity analysis on the variation of the remuneration applied to floating wind energy and floating solar energy and resulting a) NPV and b) optimal PV power to be installed in the second hybrid scenario.

remuneration scenarios. When the solar remuneration approaches the wind remuneration (125 and 165 €/MWh, respectively), it becomes convenient to add 800 MW of solar energy to maximize the NPV, even if 25 % of solar energy is wasted. The extra solar energy quickly rises to 1.1 GW when both sources receive 145 €/MWh, but stabilizes at 1.2 and 1.3 GW even when the equal remuneration rises to 165 and 185 €/MWh, respectively. This saturation point corresponds again to the change in the slope of the solar curtailment curve in Fig. 14.

Results from the second scenario are consistent with the findings from Golroodbari et al. [19]. The concept of "cable pooling" proved to be beneficial in technical terms, and in market scenarios in which the remuneration for FPV makes the technology economically viable. In the North Sea case they considered, adding up to 1.9 GWp of FPV to a 752 MW fixed-bottom wind farm connected through a 700 MW export cable increases the cable capacity factor from around 50 % (wind-only) to 88 %, while PV curtailment remains around 5 % even when PV capacity is similar to the wind capacity. The anti-correlation between wind and solar energy is lower in the considered Sicilian site. The 1 GW export cable starts from a lower utilization (41.6 % with wind only) and reaches about 56 % when 1.13 GW of FPV is installed (Fig. 15), while PV curtailment rises to 23.6 % for a PV-to-wind ratio of 0.6 and to 30–45 % when PV capacity approaches 1.25–2.0 times the wind capacity. Despite these less favorable conditions, the present analysis still demonstrates that this strategy remains effective when applied to southern European sites.

From an economic perspective, results show that cable pooling becomes attractive only under favorable FPV cost and support conditions. Results from Ref. [19] report positive NPV without subsidies only when FPV specific CAPEX is comparable with land-based PV, whereas the present work identifies an FPV cost threshold of about 1.11 M€/MW under the FER2 remuneration, above which hybrid configurations become unprofitable despite the higher cable utilization. Compared to the North Sea case, the present work therefore quantifies a stricter FPV cost threshold for economic viability, reflecting both the different resource complementarity and the FER2 remuneration structure.

Technical benefits arising from the shared use of the export cable are also in line with findings from Kazemi-Robati et al. [20]. For the three case studies considered in Ref. [20], optimal hybrid configurations supported by incentives between 25 % and 75 % on top of the wholesale price reach expected cable capacity factors above 60 % and keep curtailed energy below 15 % of the total generation. In the present case study, the FPV remuneration threshold at which hybridization becomes attractive corresponds to similar utilization rates of the export cable and shares of curtailed energy. This result indicates that comparable levels of incentives could make cable pooling economically convenient also for fully floating wind–solar plants in southern European conditions.

5. Conclusions

This paper investigated hybrid offshore energy systems comprising floating wind turbines and floating solar PV panels. The work applied a simulation method able to compute the time-varying production from wind and solar generators and to consider the temporal match between the two sources.

Two scenarios were presented, referring to a case study in Italy, for which actual prices for the two technologies at hand are now available. The first one considers hybrid farms with a total rated power capacity of 1 GW, varying the wind and solar share in the mix, and the second one, in which the solar production is added to a fixed 1-GW wind farm, keeping the maximum power export to shore equal to 1 GW and curtailing the excess.

The power production from floating solar panels was estimated using a series of functions and libraries from pvlib, while layouts of wind farms were optimized using TOPFARM, and the time-dependent wind generation was obtained using PyWake.

With an FPV price higher than 1.11 M€/MW, the LCOE of solar energy becomes higher than the remuneration proposed by FER2 (105 €/MWh). This makes the installation of FPV unfeasible from an economic point of view for every case scenario considered in this study. Differently, when considering a low FPV price from optimistic projections (0.91 M€/MW), farms comprising only solar energy would be characterized by a considerably lower LCOE (88.8 €/MWh) than farms based only on wind energy (137.6 €/MWh). Even in this case, due to the double energy production of wind generators and the much higher remuneration proposed (+80€/MWh), offshore wind energy is the best choice to maximize earnings (2.13 B€ vs 0.32 B€).

When both sources are remunerated equally in the first scenario, the optimal configuration is shifted towards solar-oriented farms (lower LCOE), but the wind share rises with the increase in the remuneration (higher AEP).

The introduction of additional solar power to a 1 GW wind farm is beneficial from a technical point of view, even if excess solar energy must be curtailed, but is again financially feasible only when considering the lower FPV price. Concerning the stand-alone installation of a 1 GW wind farm, a system that adds 595 MW of FPV can increase the utilization factor of the export cable (+8.2 %) and maximize the NPV (+2.8 %). A higher remuneration for FPV makes the extra solar energy even more competitive at power levels up to 1.3 GW, corresponding to the point at which the cable starts acting as a bottleneck and the slope of the solar-curtailed curve changes.

The specific results of the case study under consideration were also critically compared with findings from the literature. The comparison suggests that support schemes driving cable capacity factors above 60 % while keeping curtailment below roughly 15–25 % can be indicated as practical targets for making cable pooling economically viable. Overall, the comparison with previous studies shows that, although the Sicilian site exhibits weaker wind–solar complementarity and higher curtailment than northern locations, cable pooling can still increase cable utilization by about 15 percentage points. The present analysis adds to the literature by extending these findings to fully floating wind–solar farms in southern European seas and by identifying explicit FPV cost and remuneration thresholds for economically optimal hybridization.

Results have highlighted many criticalities behind the installation of FPV, showing the stakeholders in the Mediterranean area that there is a need to propose new incentives to push forward the installation of RES in offshore environments, key to differentiating the energy production and reducing grid congestion.

CRediT authorship contribution statement

Francesco Superchi: Writing – original draft, Visualization, Validation, Software, Methodology, Investigation, Formal analysis, Data curation, Conceptualization. **Riccardo Travaglini:** Writing – review & editing, Software, Methodology, Formal analysis, Conceptualization. **Alessandro Bianchini:** Writing – review & editing, Visualization, Supervision, Resources, Methodology, Funding acquisition, Formal analysis, Conceptualization.

Declaration of competing interest

The authors declare that they have no known competing financial interests or personal relationships that could have appeared to influence the work reported in this paper.

Appendix

This section provides additional material that complements the description of the methods and supports the interpretation of the results presented in Section 4.

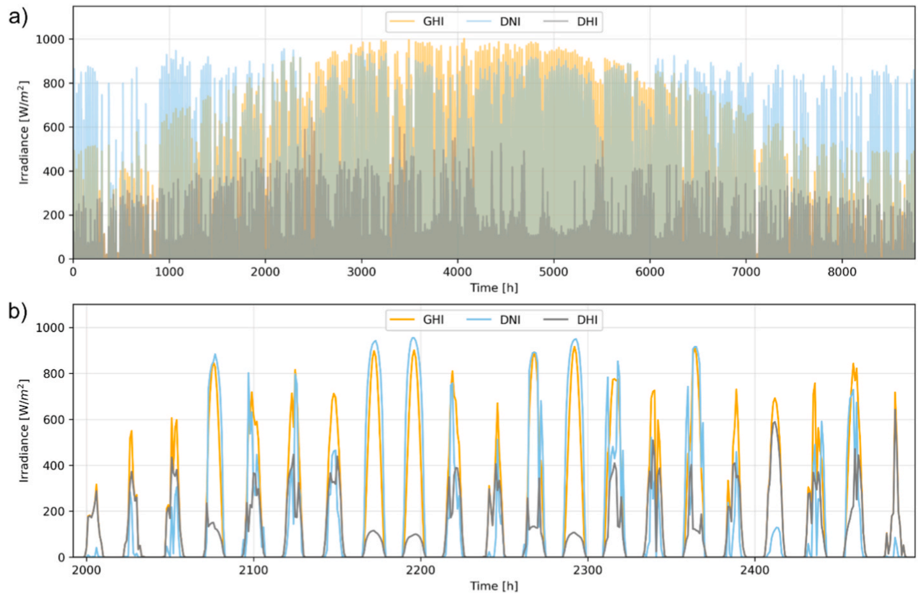

Fig. A 1. a) Trend of GHI, DNI, and DHI during the typical year and b) zoom on three weeks.

Figure A 1 shows the time-series used to compute the time-varying power production from FPV. Figure A 1 (a) reports the full trend of GHI, DNI, and DHI during a TMY for solar irradiance. Figure A 1 (b) zooms on three weeks of operation to highlight the difference between the three irradiance components.

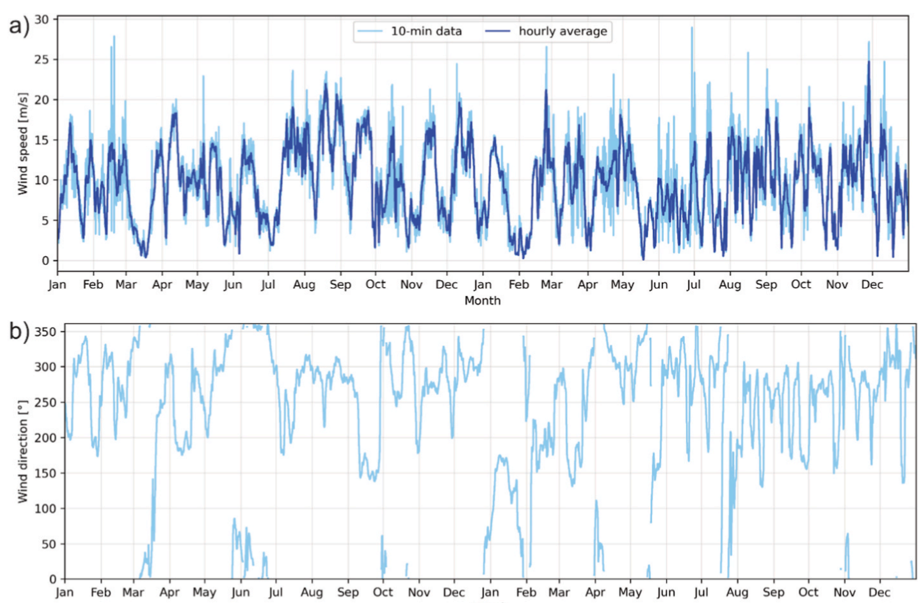

Fig. A 2. a) Wind speed trend (10-min and 1-h) and b) wind direction over the two years considered for the analysis used for the time-dependent analyses.

Figure A 2 shows the time-series used to compute the time-varying power production from the floating wind farm. The dark blue line in Figure A 2 (a) represents the original 1-h trend obtained from ERA5, while the light blue line is the 10-min trend computed following the procedure described in Section 3.2. The wind direction trend is reported in Figure A 2 (b) in degrees, where the zero represents the North.

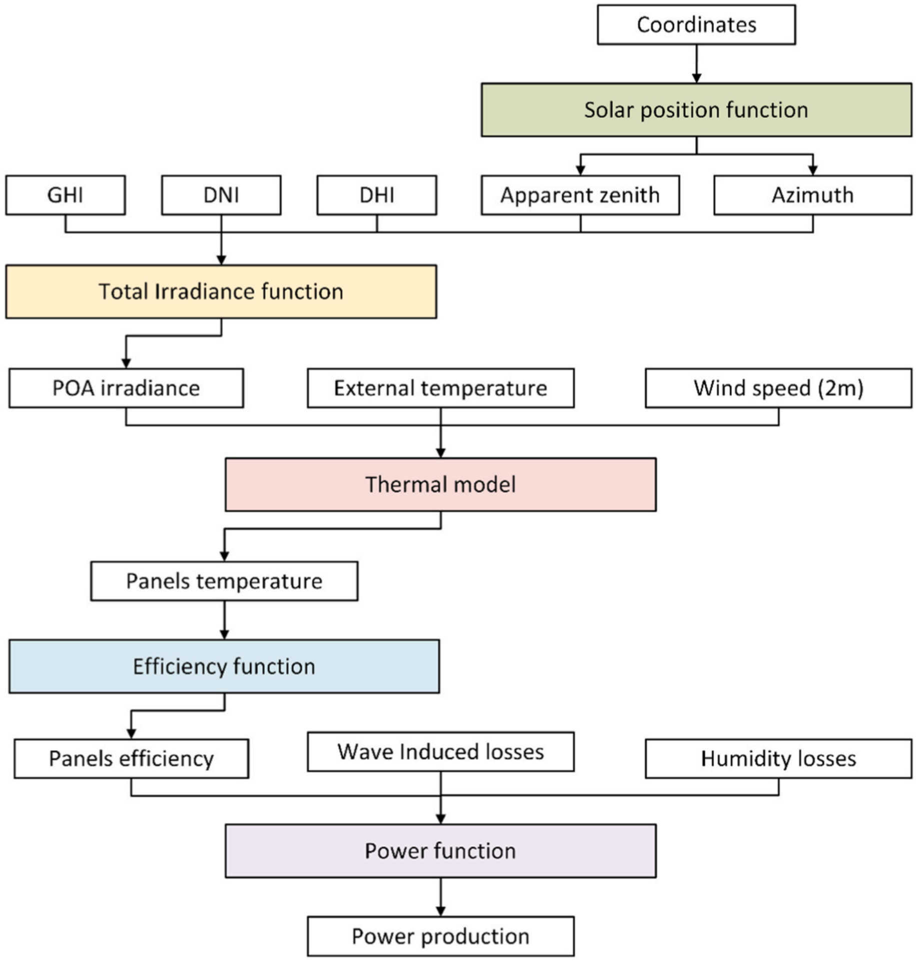

Fig. A 3. Flowchart of the mathematical model for the estimation of the power production from FPV

Figure A 3 schematizes the mathematical model used to obtain the power production of the FPV array. The flowchart clarifies which data serve as inputs to each block and how these blocks are interconnected. The model uses several functions from the pvlib Python package.

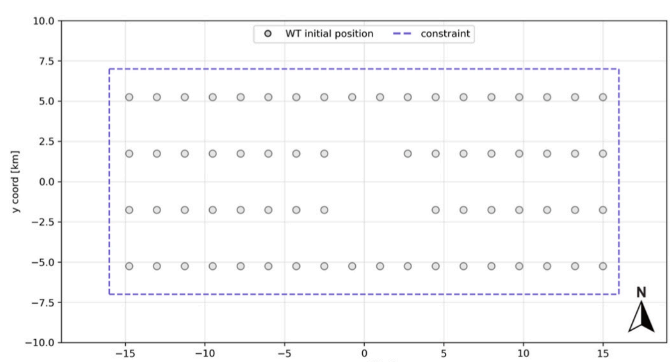

Fig. A 4. Initial layout of a 1 GW wind farm comprising sixty-seven 15 MW wind turbines.

Figure A 4 shows the initial layout of wind turbines considered by TOPFARM (Section 3.4) in the case of the 1 GW wind farm comprising sixty-seven generators. The initial layout consists in homogeneously distributed points in the available sea lot (dashed line). A free area in the central part of the space is reserved for the positioning of the electrical substation and, in hybridized scenarios, the FPV array.

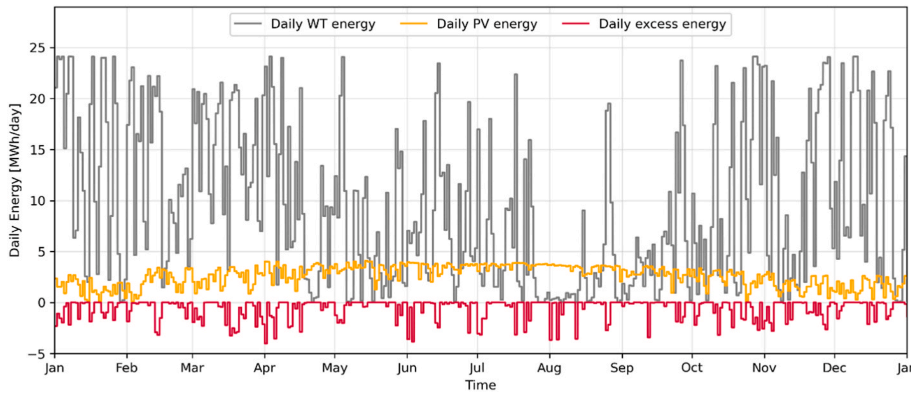

Fig. A 5. Comparison between the daily energy production from a 1 GW wind farm and a 600 MW FPV field and curtailed energy when the systems are sharing the same 1 GW export cable.

Figure A 5 shows the comparison between the daily energy production from a 1 GW wind farm (grey line) and a 600 MW FPV field (orange line) and curtailed energy (red line) when the systems are sharing the same 1 GW export cable. The direct comparison between the two energy generation trends shows that the anti-correlation between the two sources limits the power curtailment applied to the cheapest energy source. The higher winter production from wind turbines and the higher summer production from FPV increase the power output stability of the system.

Table A
Rated power, AEP, CF, and wake losses of the sixty-seven layout optimizations performed.

n° WTs	Power [MW]	AEP [GWh]	CF [%]	WL [%]	n° WTs	Power [MW]	AEP [GWh]	CF [%]	WL [%]
1	15	54	41.1	0	35	525	1848.5	40.2	2.47
2	30	107.8	41	0.5	36	540	1899.4	40.2	2.57
3	45	161.1	40.9	0.84	37	555	1951.7	40.1	2.59
4	60	214.4	40.8	1.03	38	570	2002.4	40.1	2.69
5	75	267.6	40.7	1.18	39	585	2054.4	40.1	2.72
6	90	320.8	40.7	1.26	40	600	2107	40.1	2.72
7	105	373.8	40.6	1.38	41	615	2156.9	40	2.85
8	120	427	40.6	1.44	42	630	2209.4	40	2.85
9	135	480.4	40.6	1.43	43	645	2263.2	40.1	2.8
10	150	533.5	40.6	1.48	44	660	2312.2	40	2.95
11	165	586.5	40.6	1.54	45	675	2363.8	40	2.99
12	180	639.9	40.6	1.53	46	690	2417.2	40	2.96
13	195	693.1	40.6	1.55	47	705	2469.7	40	2.96
14	210	746.3	40.6	1.56	48	720	2522.2	40	2.96
15	225	799.3	40.6	1.59	49	735	2571.8	39.9	3.07
16	240	852.7	40.6	1.58	50	750	2618.2	39.9	3.3
17	255	906.3	40.6	1.55	51	765	2672.2	39.9	3.24
18	270	959.5	40.6	1.56	52	780	2725.4	39.9	3.21
19	285	1012.3	40.5	1.61	53	795	2774.9	39.8	3.31
20	300	1063.7	40.5	1.78	54	810	2824.2	39.8	3.41
21	315	1116.8	40.5	1.79	55	825	2878	39.8	3.37
22	330	1170	40.5	1.79	56	840	2926.9	39.8	3.48
23	345	1222.5	40.5	1.84	57	855	2981.7	39.8	3.4
24	360	1275.6	40.4	1.85	58	870	3027.8	39.7	3.59
25	375	1327.1	40.4	1.97	59	885	3078.9	39.7	3.63
26	390	1379.7	40.4	2	60	900	3137.5	39.8	3.43
27	405	1430.8	40.3	2.14	61	915	3187.5	39.8	3.5
28	420	1485.2	40.4	2.04	62	930	3237.5	39.7	3.57
29	435	1538.2	40.4	2.05	63	945	3288.8	39.7	3.6
30	450	1590.2	40.3	2.11	64	960	3340.7	39.7	3.6
31	465	1639.3	40.2	2.35	65	975	3387	39.7	3.77
32	480	1694.4	40.3	2.22	66	990	3444.8	39.7	3.61
33	495	1744.5	40.2	2.38	67	1005	3494.3	39.7	3.69
34	510	1797.7	40.2	2.36					

Table A reports the main results in terms of AEP, CF, and wake losses from the sixty-seven layout optimizations performed. Results related to an incremental number of wind turbines included in the floating farm are used to assess the techno-economic outcome of hybrid wind-solar systems considered for the first scenario (Section 4.3).

References

[1] R. Travaglini, L.S.F. Frowijn, A. Bianchini, Z. Lukszo, K. Bruninx, Offshore or onshore hydrogen production? A critical analysis on costs and operational considerations for the Dutch North Sea, Appl. Energy 397 (2025) 126290, https://doi.org/10.1016/j.apenergy.2025.126290.

[2] B. Morin, Far A. Maimó, D. Flynn, C. Sweeney, Reducing RES droughts through the integration of wind and solar PV, Renew. Energy 252 (2025) 123392, https://doi.org/10.1016/j.renene.2025.123392.

[3] X. Yuan, Y. Wei, H. Yang, Does the ocean have better suitability for wind–solar energy complementarity than land? A regional study in East Asia, Renew. Energy 250 (2025) 123207, https://doi.org/10.1016/j.renene.2025.123207.

[4] R. Vázquez, W. Cabos, J.C. Nieto-Borge, C. Gutiérrez, Complementarity of offshore energy resources on the Spanish coasts: wind, wave, and photovoltaic energy, Renew. Energy 224 (2024) 120213, https://doi.org/10.1016/j.renene.2024.120213.
[5] M. López, N. Rodríguez, G. Iglesias, Combined floating offshore wind and solar PV, J. Mar. Sci. Eng. 8 (2020) 576, https://doi.org/10.3390/jmse8080576.
[6] H. Jiang, L. Yao, C. Zhou, Assessment of offshore wind-solar energy potentials and spatial layout optimization in mainland China, Ocean Eng 287 (2023) 115914, https://doi.org/10.1016/j.oceaneng.2023.115914.
[7] F. Ali, A. Etemad-Shahidi, R.A. Stewart, M.J. Sanjari, J.A. Hayward, R. C. Nicholson, Co-located offshore wind and floating solar farms: a systematic quantitative literature review of site selection criteria, Renew. Energy Focus 50 (2024) 100611, https://doi.org/10.1016/j.ref.2024.100611.
[8] X. Costoya, M. deCastro, D. Carvalho, B. Arguilé-Pérez, M. Gómez-Gesteira, Combining offshore wind and solar photovoltaic energy to stabilize energy supply under climate change scenarios: a case study on the western Iberian Peninsula, Renew. Sustain. Energy Rev. 157 (2022) 112037, https://doi.org/10.1016/j.rser.2021.112037.
[9] C. Bi, A.W.-K. Law, Co-locating offshore wind and floating solar farms – effect of high wind and wave conditions on solar power performance, Energy 266 (2023) 126437, https://doi.org/10.1016/j.energy.2022.126437.
[10] M.M. de Souza Nascimento, M. Shadman, C. Silva, L.P. de Freitas Assad, S. F. Estefen, L. Landau, Offshore wind and solar complementarity in Brazil: a theoretical and technical potential assessment, Energy Convers. Manag. 270 (2022) 116194, https://doi.org/10.1016/j.enconman.2022.116194.
[11] L. Frías-Paredes, M. Gastón-Romeo, A new methodology to easy integrate complementarity criteria in the resource assessment process for hybrid power plants: offshore wind and floating PV, Energy Convers. Manag. X 26 (2025) 100938, https://doi.org/10.1016/j.ecmx.2025.100938.
[12] J. Liu, X. Ma, C. Lu, A three-stage framework for optimal site selection of hybrid offshore wind-photovoltaic-wave-hydrogen energy system: a case study of China, Energy 313 (2024) 133723, https://doi.org/10.1016/j.energy.2024.133723.
[13] H. Khurshid, B.S. Mohammed, A.M. Al-Yacouby, M.S. Liew, N.A.W.A. Zawawi, Analysis of hybrid offshore renewable energy sources for power generation: a literature review of hybrid solar, wind, and waves energy systems, Dev. Built Environ. 19 (2024) 100497, https://doi.org/10.1016/j.dibe.2024.100497.
[14] J. Huang, G. Iglesias, Hybrid offshore wind–solar energy farms: a novel approach through retrofitting, Energy Convers. Manag. 319 (2024) 118903, https://doi.org/10.1016/j.enconman.2024.118903.
[15] M.H. Jahangir, A. Shahsavari, M.A. Vaziri Rad, Feasibility study of a zero emission PV/Wind turbine/Wave energy converter hybrid system for stand-alone power supply: a case study, J. Clean. Prod. 262 (2020) 121250, https://doi.org/10.1016/j.jclepro.2020.121250.
[16] M.H. Jahangir, S. Fakouriyan, M.A. Vaziri Rad, H. Dehghan, Feasibility study of on/off grid large-scale PV/WT/WEC hybrid energy system in coastal cities: a case-based research, Renew. Energy 162 (2020) 2075–2095, https://doi.org/10.1016/j.renene.2020.09.131.
[17] S. Kumar, N. Panagant, E. Arzaghi, T. Baalisampang, V. Garaniya, R. Abbassi, A multi-objective optimisation framework for a standalone hybrid offshore renewable energy system with electrical and hydrogen loads, Energy 330 (2025) 136826, https://doi.org/10.1016/j.energy.2025.136826.
[18] O. Delbeke, J.D. Moschner, J. Driesen, The complementarity of offshore wind and floating photovoltaics in the Belgian North Sea, an analysis up to 2100, Renew. Energy 218 (2023) 119253, https://doi.org/10.1016/j.renene.2023.119253.
[19] S.Z.M. Golroodbari, D.F. Vaartjes, J.B.L. Meit, A.P. van Hoeken, M. Eberveld, H. Jonker, et al., Pooling the cable: a techno-economic feasibility study of integrating offshore floating photovoltaic solar technology within an offshore wind park, Sol. Energy 219 (2021) 65–74, https://doi.org/10.1016/j.solener.2020.12.062.
[20] E. Kazemi-Robati, B. Silva, R.J. Bessa, Stochastic optimization framework for hybridization of existing offshore wind farms with wave energy and floating photovoltaic systems, J. Clean. Prod. 454 (2024) 142215, https://doi.org/10.1016/j.jclepro.2024.142215.
[21] L. Serri, M.A. Peviani, S. Alborghetti, S. Milani, Valutazioni di Produzione Combinata Di Energia Elettrica Da Onde E Vento Nel Sito Della Boa MOBI Nel Canale Di Sicilia, 2021.
[22] R. Travaglini, F. Superchi, A. Bianchini, Mitigating curtailments in offshore wind energy: a comparative analysis of new and second-life battery storage solutions, J. Clean. Prod. 519 (2025) 146055, https://doi.org/10.1016/j.jclepro.2025.146055.
[23] G.M. Tina, F. Bontempo Scavo, L. Merlo, F. Bizzarri, Comparative analysis of monofacial and bifacial photovoltaic modules for floating power plants, Appl. Energy 281 (2021) 116084, https://doi.org/10.1016/j.apenergy.2020.116084.
[24] A. Ghigo, E. Faraggiana, M. Sirigu, G. Mattiazzo, G. Bracco, Design and analysis of a floating photovoltaic System for offshore installation: the case Study of Lampedusa, Energies 15 (2022) 8804, https://doi.org/10.3390/en15238804.
[25] K.S. Anderson, C.W. Hansen, W.F. Holmgren, A.R. Jensen, M.A. Mikofski, A. Driesse, Pvlib python: 2023 project update, J. Open Source Softw. 8 (2023) 5994, https://doi.org/10.21105/joss.05994.
[26] R. Kumar, M.A. Rosen, A critical review of photovoltaic–thermal solar collectors for air heating, Appl. Energy 88 (2011) 3603–3614, https://doi.org/10.1016/j.apenergy.2011.04.044.
[27] V.S. Nysted, L.E.S. Stieng, M. Kumar, N. Roosloot, G. Otnes, T. Kjeldstad, et al., Modelling wave-induced losses for floating photovoltaics: impact of design parameters and environmental conditions, Sol. Energy 293 (2025) 113439, https://doi.org/10.1016/j.solener.2025.113439.
[28] A. Goswami, Effect of humidity on the generation capacity of floating solar photovoltaic system, Jordan J Electr Eng 9 (2023) 31, https://doi.org/10.5455/jjee.204-1667584023.
[29] S. Kichou, N. Skandalos, P. Wolf, Floating photovoltaics performance simulation approach, Heliyon 8 (2022) e11896, https://doi.org/10.1016/j.heliyon.2022.e11896.
[30] IEA Wind, IEA Wind TCP Task 37, Definition of the IEA Wind 15-Megawatt Offshore Reference Wind Turbine, 2020.
[31] Riva R, Liew JY, Friis-Møller M, Krasimirov Dimitrov N, Barlas E, Réthoré P-E, et al. Welcome to TOPFARM n.d. https://topfarm.pages.windenergy.dtu.dk/TopFarm2/index.html (accessed February 11, 2025).
[32] R. Travaglini, F. Papi, A. Bianchini, Floating wind farms in sea basins with moderate wind speeds: a critical assessment of the potential of low-specific-power turbines in reducing the LCoE, Renew. Sustain. Energy Rev. 222 (2025) 115990, https://doi.org/10.1016/j.rser.2025.115990.
[33] M. Mads, , Pedersen BTO Alexander Meyer Forsting, Paul van der Laan, Riccardo Riva, Leonardo A. Alcayaga Romàn, Javier Criado Risco, Mikkel Friis-Møller, Julian Quick, Jens Peter Schøler Christiansen, Rafael Valotta Rodrigues, P.-E. Réthoré, Pywake 2.5.0: an open-source Wind Farm Simulation Tool, 2023.
[34] B.W. Yan, Q.S. Li, P.W. Chan, Y.C. He, Z.R. Shu, Characterising wind shear exponents in the offshore area using Lidar measurements, Appl. Ocean Res. 127 (2022) 103293, https://doi.org/10.1016/j.apor.2022.103293.
[35] G. Froese, S.Y. Ku, A.C. Kheirabadi, R. Nagamune, Optimal layout design of floating offshore wind farms, Renew. Energy 190 (2022) 94–102, https://doi.org/10.1016/j.renene.2022.03.104.
[36] R. Travaglini, F. Superchi, F. Lanni, G. Manzini, L. Serri, A. Bianchini, Feasibility study on the use of large-scale lithium-ion batteries to prevent energy wastes due to curtailments in offshore wind farms. https://doi.org/10.52202/077185, 2024.
[37] DTU Cost Model — TOPFARM 2.5.0.post4 documentation n.d. https://topfarm.pages.windenergy.dtu.dk/TopFarm2/api_reference/dtucost.html. (Accessed 12 February 2025).
[38] GSE, FER 2: la nuova misura per Impianti Innovativi a Fonti Rinnovabili. https://www.gse.it/servizi-per-te/fonti-rinnovabili/fer2, 2024. (Accessed 12 February 2025).
[39] A. Niccolai, F. Grimaccia, G.D. Lorenzo, R. Araneo, F. Ughi, M. Polenghi, A review of floating PV systems with a techno-economic analysis, IEEE J Photovolt 14 (2024) 23–34, https://doi.org/10.1109/JPHOTOV.2023.3319601.
[40] IRENA, Renewable power generation costs in 2020, International Renewable Energy Agency (2021).
[41] V. Ramasamy, R. Margolis, Floating Photovoltaic System Cost Benchmark: Q1 2021 Installations on Artificial Water Bodies, National Renewable Energy Lab. (NREL), Golden, CO (United States), 2021, https://doi.org/10.2172/1828287.
[42] AERO, Position Paper: Il Fotovoltaico Galleggiante Offshore per L'Italia, Associazione delle Energie RinnovabiliOffshore, 2025.
[43] S. Jalili, S.R. Cauvin, M. Kapitaniak, R. Neilson, Multi-criteria decision-making for offshore wind farm decommissioning: lessons from the oil and gas sector, Appl. Energy 399 (2025) 126529, https://doi.org/10.1016/j.apenergy.2025.126529.